JOURNAL OF GEOPHYSICAL RESEARCH, VOL. 112, D11202, doi:10.1029/2006JD008003, 2007



# Present-day climate forcing and response from black carbon in snow

Mark G. Flanner,[1] Charles S. Zender,[1] James T. Randerson,[1] and Philip J. Rasch[2]

Received 7 September 2006; revised 27 November 2006; accepted 30 January 2007; published 5 June 2007.

[1] We apply our Snow, Ice, and Aerosol Radiative (SNICAR) model, coupled to a general circulation model with prognostic carbon aerosol transport, to improve understanding of climate forcing and response from black carbon (BC) in snow. Building on two previous studies, we account for interannually varying biomass burning BC emissions, snow aging, and aerosol scavenging by snow meltwater. We assess uncertainty in forcing estimates from these factors, as well as BC optical properties and snow cover fraction. BC emissions are the largest source of uncertainty, followed by snow aging. The rate of snow aging determines snowpack effective radius ($r_e$), which directly controls snow reflectance and the magnitude of albedo change caused by BC. For a reasonable $r_e$ range, reflectance reduction from BC varies threefold. Inefficient meltwater scavenging keeps hydrophobic impurities near the surface during melt and enhances forcing. Applying biomass burning BC emission inventories for a strong (1998) and weak (2001) boreal fire year, we estimate global annual mean BC/snow surface radiative forcing from all sources (fossil fuel, biofuel, and biomass burning) of +0.054 (0.007–0.13) and +0.049 (0.007–0.12) W $m^{-2}$, respectively. Snow forcing from only fossil fuel + biofuel sources is +0.043 W $m^{-2}$ (forcing from only fossil fuels is +0.033 W $m^{-2}$), suggesting that the anthropogenic contribution to total forcing is at least 80%. The 1998 global land and sea-ice snowpack absorbed 0.60 and 0.23 W $m^{-2}$, respectively, because of direct BC/snow forcing. The forcing is maximum coincidentally with snowmelt onset, triggering strong snow-albedo feedback in local springtime. Consequently, the "efficacy" of BC/snow forcing is more than three times greater than forcing by $CO_2$. The 1998 and 2001 land snowmelt rates north of 50°N are 28% and 19% greater in the month preceding maximum melt of control simulations without BC in snow. With climate feedbacks, global annual mean 2-meter air temperature warms 0.15 and 0.10°C, when BC is included in snow, whereas annual arctic warming is 1.61 and 0.50°C. Stronger high-latitude climate response in 1998 than 2001 is at least partially caused by boreal fires, which account for nearly all of the 35% biomass burning contribution to 1998 arctic forcing. Efficacy was anomalously large in this experiment, however, and more research is required to elucidate the role of boreal fires, which we suggest have maximum arctic BC/snow forcing potential during April–June. Model BC concentrations in snow agree reasonably well ($r = 0.78$) with a set of 23 observations from various locations, spanning nearly 4 orders of magnitude. We predict concentrations in excess of 1000 ng $g^{-1}$ for snow in northeast China, enough to lower snow albedo by more than 0.13. The greatest instantaneous forcing is over the Tibetan Plateau, exceeding 20 W $m^{-2}$ in some places during spring. These results indicate that snow darkening is an important component of carbon aerosol climate forcing.

**Citation:** Flanner, M. G., C. S. Zender, J. T. Randerson, and P. J. Rasch (2007), Present-day climate forcing and response from black carbon in snow, *J. Geophys. Res.*, *112*, D11202, doi:10.1029/2006JD008003.

## 1. Introduction

[2] Very small quantities of black carbon (BC, the strongly absorbing component of carbonaceous aerosols) reduce snow reflectance because of multiple scattering in the snowpack and huge disparity between mass absorption coefficients of BC and ice [e.g., *Warren and Wiscombe*, 1980]. Reflectance reduction caused by BC and other absorbing impurities is of concern because slight changes

[1] Department of Earth System Science, University of California, Irvine, California, USA.
[2] National Center for Atmospheric Research, Boulder, Colorado, USA.


0148-0227/07/2006JD008003$09.00

in solar absorption can alter snowmelt timing, and snow spatial coverage is tightly coupled to climate through snow-albedo feedback [e.g., *Budyko*, 1969].

[3] Several other positive feedbacks amplify the first-order warming effect of BC in snow. Warmer snow temperatures can accelerate snow effective radius ($r_e$) growth [e.g., *Flanner and Zender*, 2006], which darkens the snow itself. Second, the radiative perturbation of a given BC mass mixing ratio is greater in snow with larger $r_e$ [*Warren and Wiscombe*, 1980]. Third, spring and summer melting can concentrate hydrophobic and large impurities near the snow surface [*Clarke and Noone*, 1985]. Fourth, the stable atmosphere of high latitudes prevents rapid heat exchange with the upper troposphere, resulting in strong surface temperature response to surface radiative forcings [*Hansen and Nazarenko*, 2004]. We represent all of these feedbacks with a coupled snow-aerosol-climate model.

[4] *Hansen and Nazarenko* [2004] raised awareness of BC/snow forcing by assuming spatially uniform snow albedo reductions over arctic sea-ice and Northern Hemisphere land. They estimate global adjusted BC/snow radiative forcing of +0.15 W $m^{-2}$, and global warming of 0.24°C, yielding a forcing "efficacy" [*Hansen et al.*, 2005], or change in equilibrium global mean temperature per unit power of radiative forcing, double that of $CO_2$. *Hansen et al.* [2005] scaled the BC/snow forcing based on deposition fields and revised their original estimate to +0.05 W $m^{-2}$ (corrected value published in Appendix A.5 in *Hansen et al.* [2007]), with a warming of 0.065°C. *Jacobson* [2004b] predicts snow and ice reflectance with a radiative transfer solution that interactively depends on BC deposition in an aerosol/chemical transport general circulation model (GCM). He predicts warming of 0.06°C from snow darkening by fossil fuel and biofuel BC.

[5] We attempt to build upon these studies by accounting for, and assessing uncertainty from interannually varying biomass burning BC emissions, snow aging and spatially varying grain size, meltwater scavenging of BC in the snowpack, BC optical properties, and snow cover fraction. We discuss some features of our Snow, Ice, and Aerosol Radiative (SNICAR) model, including the influence of snow $r_e$ on reflectance and vertical heating perturbation from BC. Next we compare global predictions of BC in snow with observations. Then we estimate the global climate response and efficacy of BC/snow forcing, finding threefold greater global temperature response than expected from equal forcing by $CO_2$. Finally, we look at spatial and temporal patterns of the forcing and climate response with the goal of understanding this large efficacy in the context of snowmelt timing and snow-albedo feedback.

## 2. Methods

[6] We simulate radiative transfer in the snowpack with SNICAR [*Flanner and Zender*, 2005], which utilizes theory from *Wiscombe and Warren* [1980] and the two-stream, multilayer radiative approximation of *Toon et al.* [1989]. The multilayer model allows for vertically heterogeneous snow properties and heating, and influence of surfaces underlying snowpack. We couple this snow radiative model to the National Center for Atmospheric Research (NCAR) Community Atmosphere Model, version 3 (CAM3) [e.g., *Collins et al.*, 2004], with configuration described below.

[7] Hemispheric radiative fluxes may be accurately estimated for media composed of aspherical ice particles by assuming collections of spheres that conserve the total surface area and volume of the real media [*Grenfell and Warren*, 1999; *Neshyba et al.*, 2003; *Grenfell et al.*, 2005]. For this reason, $r_e$, or surface area-weighted mean radius, is the most appropriate snow grain metric for optical considerations. We compute Mie parameters off-line at fine spectral resolution for lognormal distributions of absorbing aerosols and a wide range of ice $r_e$. Coupled to a GCM, SNICAR uses only five spectral bands (0.3–0.7, 0.7–1.0, 1.0–1.2, 1.2–1.5, and 1.5–5.0 $\mu$m) for computational efficiency. Following the Chandrasekhar mean approach, optical properties are weighted into broadbands according to incident solar flux [*Thomas and Stamnes*, 1999]. We use surface incident flux typical of midlatitude winter for clear- and cloudy-sky conditions, generated with the atmospheric Shortwave Narrowband Model (SWNB) [*Stamnes et al.*, 1988; *Zender et al.*, 1997]. In addition to weighting by solar flux, we also weight single-scatter albedo ($\omega$) for ice grains by hemispheric albedo of an optically thick snowpack:

$$\omega(\bar{\lambda}) = \frac{\int_{\lambda_1}^{\lambda_2} \omega(\lambda) S_s^{\downarrow}(\lambda) \alpha(\lambda) \mathrm{d}\lambda}{\int_{\lambda_1}^{\lambda_2} S_s^{\downarrow}(\lambda) \alpha(\lambda) \mathrm{d}\lambda} \quad (1)$$

where $S_s^{\downarrow}$ is the downwelling surface incident flux (unique for diffuse and direct cases), and $\alpha$ is the hemispheric albedo of an optically thick snowpack of homogeneous $r_e$.

[8] This weighting scheme produces relative error in albedo predicted using five bands of less than 0.5%, relative to 470-band solutions. Over a wide range of zenith angles, effective radii, and impurity concentrations, we found this technique to be significantly more accurate (factor of 5 difference in mean relative error) in predicting spectrally averaged albedo than when $\omega$ is weighted only by $S_s^{\downarrow}$. However, we stress that it is only an empirical approach and provides undesirable results in more general cases (such as the case of weighting the limits $\omega = 0$ and $\omega = 1$). It also requires a priori narrowband albedo values of the bulk medium. Errors in sub-2 cm absorption with this approach are ~4%, slightly greater than errors without the albedo weighting of $\omega$. Broadband Mie parameters for $50 \leq r_e \leq 1000$ $\mu$m are compiled into a lookup table for online retrieval in the host GCM.

[9] We partition online surface-incident visible and near-infrared (NIR), diffuse and direct flux into the five bands used by SNICAR using the same off-line estimates of narrowband midlatitude winter fluxes. We apply the delta-Eddington [*Joseph et al.*, 1976] and delta-Hemispheric Mean [*Toon et al.*, 1989] approximations in the visible and NIR spectra, respectively. In very rare situations (about 1 in $10^6$ cases), the multilayer solution approaches an indeterminate case with direct-beam incident flux [*Toon et al.*, 1989], so we adjust the Sun angle by a few degrees to achieve reasonable predictions.

[10] Multiple aerosol species are accounted for by summing extinction optical depths of each component, weighting individual single-scatter albedos by optical depths, and weighting asymmetry parameters by the product of optical

depths and single-scatter albedos. Hydrophilic and hydrophobic BC species are treated separately. Absolute error in albedo predicted with five bands for snow with BC is also <0.5%, although albedo reduction from typical BC concentrations is consistently 4–6% (relative) less with five bands than with 470. As we will show, this bias is much smaller than other uncertainties.

[11] We couple SNICAR to the CAM3 GCM with a slab ocean model that has spatially varying mixed layer depth with fixed monthly mean ocean heat transport. We include prognostic transport and wet and dry deposition of hydrophobic and hydrophilic BC and organic carbon (OC) [*Rasch et al.*, 2001], using a single size bin for each of these four components. Wet deposition tendencies consist of both first-order loss from below-cloud scavenging by precipitation and in-cloud scavenging that assumes a fixed fraction of aerosol resides within the cloud water. BC and OC dry deposition velocities are fixed at 1 mm $s^{-1}$ [e.g., *Collins et al.*, 2004]. Carbon aerosols are emitted into the atmosphere as hydrophobic and then transform to hydrophilic components with an e-folding time of 1.2 days. Transformation ceases upon deposition to the snowpack.

[12] Snow on land is represented in the Community Land Model (CLM3) [e.g., *Oleson et al.*, 2004] with a five-layer model based on *Jordan* [1991] that accounts for vertically resolved snow thermal processes, densification, and meltwater transport. Snow on sea-ice is represented with a single layer in the Community Sea Ice Model (CSIM) component of CAM3. Radiative layers in SNICAR match thermal layers in these models. GCM grid cell area is approximately 97,000 $km^2$ near the equator and 17,600 $km^2$ at 80°N.

[13] We calculate instantaneous radiative forcing of carbon aerosols in both snow and the atmosphere at each radiative transfer time step as the difference in absorbed radiation with all aerosols and all aerosols except carbon aerosols. Radiative transfer estimates with carbon aerosols feed back into the model climate. Reported atmospheric forcings are from BC + OC, whereas snow forcings are from only BC (discussed below).

[14] Forcing is sensitive to cloud treatment, which strongly affects both surface-incident and outgoing top-of-atmosphere radiative fluxes. Cloud fraction is diagnosed based on relative humidity, atmospheric stability, and convective mass fluxes [*Collins et al.*, 2004]. The cloud vertical overlap parameterization is described in *Collins* [2001]. Liquid and ice cloud optical properties are parameterized according to *Slingo* [1989] and *Ebert and Curry* [1992], respectively. Thus mixed-phase bulk cloud radiative properties depend on prognosed cloud water path [e.g., *Rasch and Kristjánsso*, 1998], temperature-dependent drop-effective radius, and ice fraction. Liquid and ice hydrometeors are each represented with a single size category. Finally, the atmospheric multilayer radiative transfer approximation [*Briegleb*, 1992] utilizes the delta-Eddington approximation and 19 spectral bands in the solar spectrum. Atmospheric and snow radiative transfers are solved separately for practical reasons, as the atmospheric radiation model is engineered to utilize predetermined surface albedo.

[15] To estimate present-day global forcing of BC in snow, we consider combinations of low, central, and high estimates of the following factors.

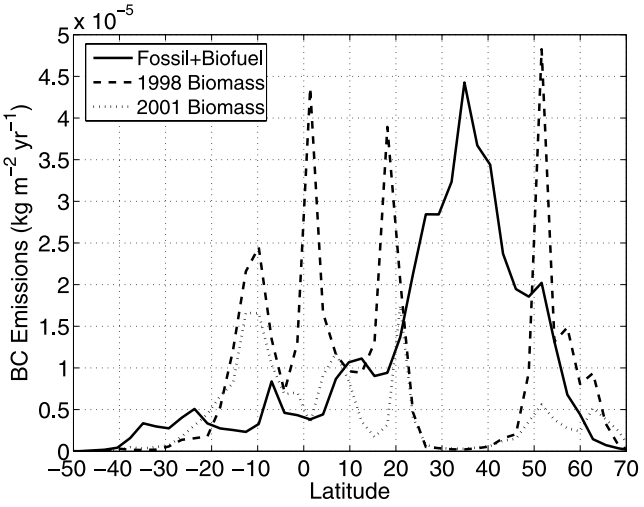


**Figure 1.** Zonal annual mean black carbon emissions from fossil fuel + biofuel combustion [*Bond et al.*, 2004] and biomass burning during 1998 and 2001 [*Van der Werf et al.*, 2006].

### 2.1. BC and OC Emissions

[16] We use low, central, and high fossil fuel (FF) and biofuel (BF) BC and OC emission estimates at 1° × 1° resolution from *Bond et al.* [2004]. These annual mean estimates are derived from 1996 fuel-use data and assumptions about local combustion technology and practice. We use monthly biomass burning (BB) estimates of BC and OC from the Global Fire Emissions Database, version 2 (GFEDv2) [*Van der Werf et al.*, 2006], which are derived from satellite-monitored burned area, modeled fuel load and combustion completeness, and aerosol emission factors from *Andreae and Merlet* [2001, personal communication]. We also apply regional satellite-derived carbon monoxide inversion factors (Prasad Kasibhatla, unpublished data, 2006), which constrain the forward emission estimates. Boreal forest fires exhibit strong interannual variability and are likely the dominant source of arctic BC during moderate fire seasons [*Stohl*, 2006]. In this 1997–2004 BB emissions time series, 1998 was the strongest boreal fire year, and we select 2001 as representative of a weak year. Boreal emissions were weaker in 1997, but global emissions were greatest this year. We estimate high and low emissions at each grid cell and month for these two years by combining standard error, in quadrature, of regional CO inversion factors and CO and BC emission factors [*Andreae and Merlert*, 2001, personal communication]. Assuming a broad range of emissions may compensate for some variability in atmospheric transport mechanisms, which we do not address here. Zonal-mean, annual FF + BF, and BB emissions are shown in Figure 1, where a large difference in high-latitude BB emissions between 1998 and 2001 can be seen. Table 1 lists global and boreal annual FF + BF and BB emission estimates, and all other experimental configurations.

[17] All emissions enter the lowest model atmosphere layer. Particulate matter from strong fires can be injected above the boundary layer, however, and assumptions about injection height may affect model high-latitude upper troposphere heating [*Rasch et al.*, 2005]. Lacking associated injection

**Table 1.** Configurations for 1998 and 2001 Low, Central, and High Experiments

| | Low Estimate | Central Estimate | High Estimate |
|---|---|---|---|
| FF + BF BC Emissions (Global/N of 30°N), Tg $yr^{-1}$ | 1.6/1.0 | 4.7/2.7 | 16.2/9.3 |
| 1998 BB BC Emissions (Global/N of 30°N), Tg $yr^{-1}$ | 2.1/0.4 | 4.1/0.8 | 6.5/1.6 |
| 2001 BB BC Emissions (Global/N of 30°N), Tg $yr^{-1}$ | 1.1/0.1 | 2.0/0.2 | 3.0/0.4 |
| BC MAC (fresh, hydrophobic), $m^2$ $g^{-1}$ at 550 nm | 6.3 | 7.5 | 8.7 |
| BC MAC (aged, hydrophilic), $m^2$ $g^{-1}$ at 550 nm | 9.5 | 11.3 | 13.1 |
| Snow Aging Scaling Factor | 0.5 | 1.0 | 2.0 |
| Snow Cover Fraction | *Oleson et al.* [2004] | *Romanov and Tarpley* [2004] | *Yang et al.* [1997] |
| Hydrophilic Meltwater Scavenging Ratio ($k_{phi}$) | 2.0 | 0.2 | 0.02 |
| Hydrophobic Meltwater Scavenging Ratio ($k_{pho}$) | 0.3 | 0.03 | 0.003 |

height information for our emission inventories, we do not assess forcing sensitivity to this factor.

### 2.2. Optical Properties

[18] *Bond and Bergstrom* [2006] comprehensively review current understanding of optical properties of freshly combusted light absorbing aerosols. They suggest a mass absorption cross section (MAC) of 7.5 ± 1.2 $m^2$ $g^{-1}$ at $\lambda = 550$ nm for uncoated particles, based mostly on samples from diesel engines and traffic tunnels. Particle density, refractive index, size distribution, coatings, and morphology all affect the optical properties. However, current understanding of these physical parameters, combined with Mie or Raleigh-Debye-Gans theory, underpredicts observed MAC by ~30% [*Bond and Bergstrom*, 2006]. Commonly used optical properties [*Hess et al.*, 1998] are in the correct observational range of BC MAC but are derived by applying Mie theory to a highly unrealistic combination of physical properties. Scattering magnitude and direction by realistic BC concentrations have negligible effect on bulk snowpack radiative transfer because scattering is dominated by the ice crystals. Therefore realistic BC MAC, even if derived with assumptions that produce unrealistic $\omega$ and scattering phase function, predicts realistic snowpack absorption enhancement. (This is not necessarily true for absorbing aerosols in the atmosphere, where scattering optical depth is much lower.) For hydrophobic BC, we use indices of refraction from *Chang and Charalampopoulos* [1990], number-median radius of 0.05 $\mu$m (a central value among many studies published in *Bond et al.* [2006]), and lognormal size distribution with geometric standard deviation of 1.5. We use particle density as a tuning parameter to obtain MAC = 7.5 $m^2$ $g^{-1}$ (±1 standard deviation from *Bond et al.* [2004] for low and high estimates) at $\lambda = 550$ nm.

[19] Coagulation between BC particles and collapse of the aggregate structure tend to occur as the particles age and obtain moisture [e.g., *Schnaiter et al.*, 2003], contributing to a reduction in MAC with atmospheric lifetime. However, particle coating from condensation of weakly absorbing material increases MAC (specific to the original BC mass) [e.g., *Jacobson*, 2001]. *Bond et al.* [2006] suggest that the net effect of these competing processes increases MAC by a factor of ~1.5 with aging. With this information, we treat aged, hydrophilic BC as sulfate coated. We apply Mie theory using the same core properties as hydrophobic BC and a sulfate coating with outer radius 1.67 times that of the uncoated BC, yielding an absorption enhancement of 1.5 at $\lambda = 550$ nm. Optical properties are applied consistently to these two aerosols in the atmosphere and snow. Uncertainty remains about BC/ice mixing states. We assume external mixtures of coated and uncoated BC, but BC coating by sulfate mimics that by ice, since both coatings are weakly absorbing. Furthermore, for small core diameters, increasing coating thickness only slightly increases the absorption amplification [*Bond et al.*, 2006].

[20] We apply OPAC optical properties [*Hess et al.*, 1998] for water-soluble aerosol to atmospheric OC [*Collins et al.*, 2002; *Cooke et al.*, 1999], but do not treat OC in the snowpack. A short GCM sensitivity study with active OC in snowpack showed global forcing 200× smaller than BC/snow forcing using these optical properties. However, several recent studies [e.g., *Bond*, 2001; *Kirchstetter et al.*, 2004; *Hoffer et al.*, 2006; *Ganguly et al.*, 2005], showing carbon aerosol absorption features with Angstrom coefficients greater than 1, and other chemical analyses led *Andreae and Gelencser* [2006] to state that, "there is clearly a substantial fraction of organic matter in fine atmospheric aerosol, which is light-absorbing, but has properties and origins very much different from soot and is definitely not black." This "brown carbon" is characterized with Angstrom coefficients from 2 to 6 and is emitted in greater quantity from biomass burning and low-temperature combustion. Future research constraining OC emissions, atmospheric processes, optical properties, and snow concentrations may show that OC is a non-negligible absorber in snowpack.

### 2.3. Snow Aging

[21] As discussed later, the change in absorbed energy caused by BC depends strongly on snow $r_e$, implying that forcing is sensitive to snow aging. We apply an empirical representation of the microphysical model developed in *Flanner and Zender* [2006], which predicts the evolution of snow specific surface area with dependence on snow temperature, temperature gradient, and density. In our model, large temperature gradients can reduce pure snow, spectrally averaged albedo by up to 0.12 within 14 days, but the influence of temperature gradient is marginalized by cold temperature and high snow density. The predictive aging equation used here is the time derivative of equation (16) in *Flanner and Zender* [2006]:

$$\frac{d\hat{S}}{dt} = \frac{1}{\kappa}\hat{S}_0\tau^{1/\kappa}(t+\tau)^{-1/\kappa-1} \quad (2)$$

where $\hat{S}$ is the snow specific surface area, $\hat{S}_0$ is the fresh snow specific surface area (assumed to be 60 $m^2$ $kg^{-1}$), $t$ is the time since snowfall (where snowfall of 10 mm liquid

water equivalent completely resets snow age and SSA), and $\kappa$ and $\tau$ are best fit parameters to predictions from the microphysical model, retrieved from a lookup table depending on local snow temperature, temperature gradient, and density. Finally, since effective radius is a surface area-weighted radius, $r_e = 3/(\hat{S}\rho_i)$, where $\rho_i$ is the bulk ice density. Model temperature gradient is taken as the mean gradient at the center of each snow layer in CLM and, for snow on sea-ice, as the temperature difference between surface air and the mean of sea-ice and snow temperatures, divided by the snow layer thickness. With a single snow layer, CSIM cannot resolve the strong temperature gradient that often exists in near-surface snow and hence likely underestimates aging. We also add a wet snow grain growth function, based on laboratory measurements, that is parameterized as a function of liquid water content [*Brun*, 1989]. Grain growth from liquid water transfer is still very poorly understood, and this function likely applies only to a limited set of snow conditions. To enable wet snow aging in CSIM, we added diagnostic prediction of liquid water content based on net energy balance of snow at the freezing temperature. Our aging parameterization does not treat effects of wind, melt-freeze cycles, and sintering. Large uncertainties remain about snow aging because of the complexity of governing processes and because few quality observational data sets exist to help understand those processes. Hence we consider half and double the rate of $r_e$ evolution predicted by SNICAR for our low and high estimates, respectively.

### 2.4. Meltwater Scavenging and Aerosol Removal

[22] Very few studies have examined meltwater scavenging of impurities in snow. CLM accounts for meltwater drainage by adding excess water to the layer beneath when liquid content exceeds the layer's holding capacity, defined by snow porosity and irreducible water saturation. We assume BC inclusion in meltwater proportional to its mass mixing ratio multiplied by a scavenging factor. Thus the BC mass rate of change in each layer $i$ is:

$$\frac{dm_i}{dt} = k(q_{i+1}c_{i+1} - q_i c_i) + D \quad (3)$$

where $m$ is the absolute mass of BC in each layer, $k$ is the scavenging ratio, $q_i$ is the mass flux of water out of layer $i$, $c_i$ is the mass mixing ratio of BC in layer $i$ (BC mass divided by liquid + solid $H_2O$ mass), and $D$ is the sum of wet and dry atmospheric deposition, added only to the surface layer. This equation has similar form to equation (2) of *Jacobson* [2004b] but is generalized for multiple snow layers and treats removal as a function of meltwater scavenging rather than with an empirical fall speed. After deposition, BC is instantly mixed uniformly in the model surface layer, which never exceeds 2-cm thickness.

[23] *Conway et al.* [1996] applied BC to the surface of melting snow and observed that 99% of hydrophilic BC and 50% of hydrophobic BC were removed from the top 50 cm of snow after 10 days. Applying a simple e-folding model with total meltwater production observed during this period, and initial and final BC mass observed in the top 2 cm, we estimate hydrophilic and hydrophobic scavenging ratios of $k_{phi} = 0.037$ and $k_{pho} = 0.031$. This estimate of $k_{phi}$ is likely too small because nearly all of the hydrophilic BC retained in the top 50 cm was in the top 2 cm, and *Conway et al.* [1996] note that particles larger than $\sim$5 $\mu$m are relatively immobile during melt. Therefore retention of hydrophilic particles near the snow surface is likely because of size rather than particle affinity for water. This is consistent with observations of mineral dust particles (typically larger than BC by 2–3 orders of magnitude) remaining near the surface during snowmelt (T. Painter, personal communication, 2006). *Conway et al.* [1996] offer unique observations of aerosol transport with snow meltwater, but the spatial and temporal resolutions of observations are too coarse, and uncertainty about the role of particle size too large, to estimate scavenging ratios with much confidence. Here we assume $k_{pho} = 0.03$, derived from observations in the top 2 cm, and apply the $k_{pho}/k_{phi}$ ratio obtained from analysis of observations in the top 50 cm of snow to obtain $k_{phi} = 0.20$. For high and low estimates, we assume an order of magnitude uncertainty (Table 1).

[24] In the absence of melt, fresh snowfall in CLM continuously divides the model surface snow layer and prevents excessive BC accumulation. In CSIM, BC accumulates excessively in snow on perennial sea-ice because of the single layer representation and because snow remains perennially on the sea-ice (an issue discussed later). Consequently, we impose empirical BC removal with an e-folding time of 1.44 years, resulting in steady state interannual concentrations. Future versions of this sea-ice model will have multiple snow layers.

### 2.5. Snow Cover Fraction

[25] Snow cover fraction (SCF) controls the area over which BC/snow forcing operates. SCF is generally parameterized as a simple function of snow depth, but also depends on orographic variability, vegetation cover, and melt/accumulation phase (Z. Liang-Yang, personal communication, 2006). We found seven widely varying SCF representations in the literature and choose the following, based solely on their relative scales, for low, central, and high SCF relationships to snow depth:

[26] • Low: SCF = $d$ / (10 $z$ + $d$) [*Oleson et al.*, 2004] (CLM)

[27] • Central: SCF = min[1.0, log(100 $d$ + 1) / 3.33] [*Romanov and Tarpley*, 2004]

[28] • High: SCF = tanh[$d$ / (2.5$z$)] [*Yang et al.*, 1997]

[29] Here $d$ is the snow depth (m) and $z$ is the surface roughness length (fixed at 0.01 m for all soil types and glacier surfaces in CLM). Snow depth of 10 cm predicts SCF of 0.47, 0.69, and 0.99 for these three representations, respectively. *Oleson et al.* [2004] is the current implementation in CLM. *Romanov and Tarpley* [2004] relates snow depth, as measured by stations in the USA and Canada, to SCF observed by satellite. Their derived relationship is valid for snow depths less than 30 cm over prairies and lightly forested regions. *Yang et al.* [1997] proposed SCF from analysis of 6 years of station data from six sites in the former Soviet Union. Improving SCF representation to account for variables other than snow depth is beyond the scope of this study.

[30] Lacking a radiative transfer approximation for BC inclusion in sea-ice, we assume snow forcing acts homogeneously over snow-covered and snow-free ice. This crude assumption probably underestimates forcing because sur-

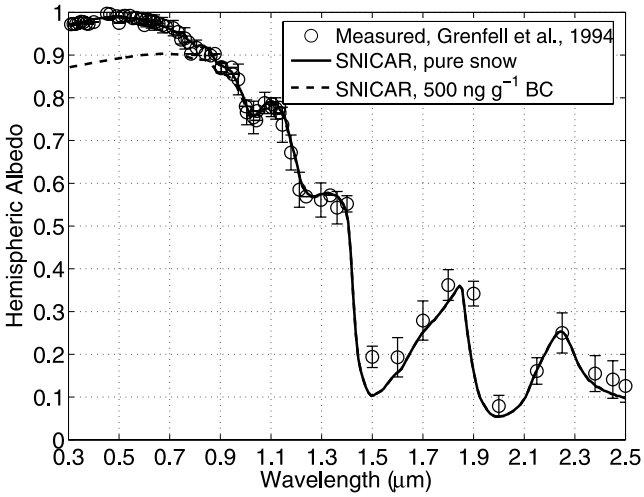


**Figure 2.** Measured diffuse incident radiation snow albedo at the South Pole from *Grenfell et al.* [1994] and modeled albedo from SNICAR assuming a 0.25 mm thick surface layer composed of 45-$\mu$m $r_e$ snow and a deep underlying layer of 100-$\mu$m $r_e$ snow. The thin surface layer controls reflectance in the highly absorptive NIR portion of the spectrum. Also shown is the modeled snow reflectance with 500 ng g$^{-1}$ of hydrophilic (coated) BC.

face sea-ice is very coarse grained [e.g., *Light et al.*, 1998] and forcing increases with increasing $r_e$.

## 3. Results and Discussion

[31] In this section, we first compare spectral albedo from SNICAR with observations and examine sensitivity of snow albedo and subsurface radiative heating to varying BC concentrations and snow effective radii. Next, we analyze GCM experiments with BC in snow, first comparing predicted BC concentrations in snow with observations, then assessing global forcing, and finally examining climate feedbacks.

### 3.1. BC Influence on Snow Albedo and Radiative Heating

[32] We first apply off-line, single-column, 470-band SNICAR to demonstrate model fidelity in reproducing observed snow reflectance. Figure 2 shows measured snow albedo for diffuse incident radiation at the South Pole (Figure 4 of *Grenfell et al.* [1994], data provided by Steve Warren) and modeled reflectance using SNICAR with a thin (0.25 mm) surface layer composed of 45-$\mu$m $r_e$ snow and a thick underlying layer composed of 100-$\mu$m $r_e$ (snow density = 350 kg m$^{-3}$). *Grenfell et al.* [1994] found that a similar two-layer model (with surface $r_e$ = 30 $\mu$m) also matched observed reflectance in both the visible and absorptive NIR. Because they did not measure snow grain size at the very high vertical resolution needed for model testing with fully known snow conditions, *Grenfell et al.* [1994] pointed out that many arbitrary layer thickness and $r_e$ model combinations can produce a good fit. Also shown in this figure is modeled albedo of the same snowpack, but with 500 ng g$^{-1}$ of hydrophilic (coated) BC. The BC strongly reduces visible reflectance, but has negligible influence at wavelengths beyond 1 $\mu$m.

[33] Next, we identify how varying concentrations of BC affect spectrally averaged (0.3–5.0 $\mu$m) hemispheric snow albedo and subsurface heating with different $r_e$. We assume an optically thick, homogeneous snowpack with direct-beam incident flux at a solar zenith angle of 60°. *Grenfell et al.* [1994] reported that, using the model of *Warren and Wiscombe* [1980], a uniform distribution of 15 ng g$^{-1}$ BC reduces albedo by 1% at 500 nm with an effective grain radius of 100 $\mu$m. In our model, hydrophobic and hydrophilic BC reduce 500 nm albedo in snow with $r_e$ = 100 $\mu$m by 0.0079 and 0.0108, respectively. The experiments discussed below apply hydrophobic BC optical properties.

[34] Figure 3 (top) shows spectrally averaged snow albedo for BC concentrations ranging from 0 to 1000 ng g$^{-1}$ and four different $r_e$. Qualitatively, these curves agree well with

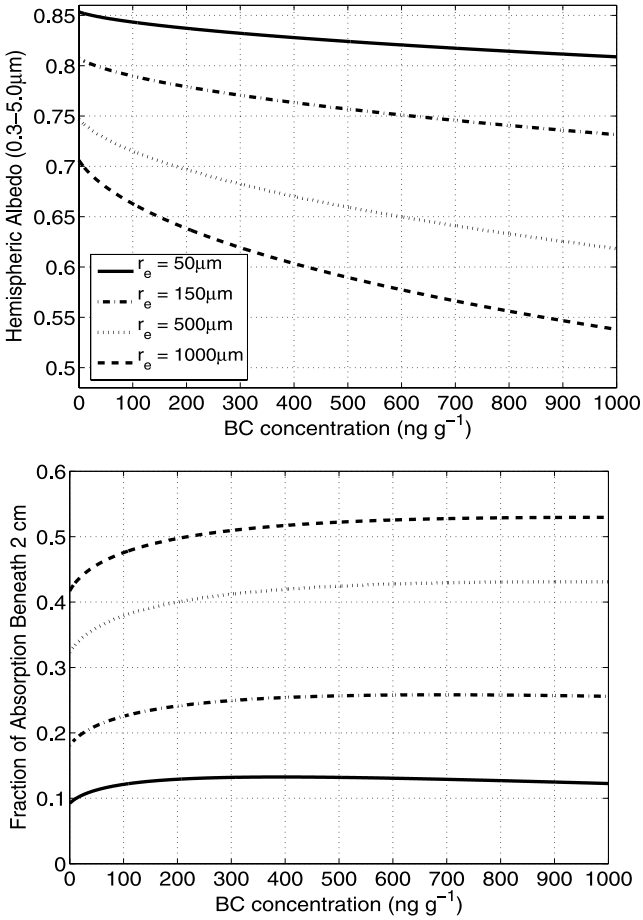


**Figure 3.** Top: Spectrally averaged snow albedo as a function of BC mass concentration for various snow effective radii ($r_e$). Note that BC perturbs albedo more in larger-grained snow. Bottom: Fraction of total snowpack absorption occurring more than 2 cm beneath the surface as a function of BC concentrations for the same $r_e$ as the top panel. Absorption occurs deeper in the snow with homogeneously mixed BC because more of the total absorption is from visible radiation, which tends to absorb deeper than NIR, even with large BC concentrations. In both experiments, the snowpack is optically semi-infinite and homogeneous. Incident flux is direct beam from 60° zenith angle. For comparison of these BC concentrations with global observations and model predictions, see Table 2 and Figures 4 and 5.

Figures 1 and 2 of *Warren and Wiscombe* [1985]. As originally noted by *Warren and Wiscombe* [1980], the presence of absorbing impurities reduces albedo more in snow with larger $r_e$. Albedo reduction for 1000 ng $g^{-1}$ BC is 0.17 and 0.045 for snow with $r_e$ = 1000 and 50 $\mu$m, respectively. Both the absolute perturbation from BC and disparity in perturbation between grain sizes grow as zenith angle decreases.

[35] The grain size effect is somewhat counterintuitive, as one naturally expects brighter media to be more susceptible to darkening by impurities. But visible radiation penetrates deeper in snow with larger $r_e$ because it has a smaller extinction coefficient and, less importantly, scatters more strongly in the forward direction. The snow depth where mean radiative intensity diminishes to 1/*e* of its surface value is 17 cm for $r_e$ = 50 $\mu$m and 78 cm for $r_e$ = 1000 $\mu$m ($\lambda$ = 550 nm, snow density = 150 kg $m^{-3}$, zenith angle = 60°). By traveling through a greater optical depth of impurities, photons thus have a greater probability of absorption by (homogeneously interspersed) impurities in snow with larger $r_e$. Sensitivity to grain size highlights the importance of snow aging treatment and realistic $r_e$, which can vary significantly on small spatial scales [*Painter et al.*, 2003].

[36] Nearly all albedo reduction from BC is due to increased absorption in the visible spectrum. NIR albedo decreases by only 0.02–0.06 with 1000 ng $g^{-1}$ BC, whereas visible albedo is reduced by 0.07–0.28 (not shown). This produces another surprising result: With homogeneously mixed BC, the fraction of total absorption occurring more than 2 cm beneath the snow surface *increases* with increasing BC amount, up to a limit. Figure 3 (bottom) shows this fraction increasing by up to 0.11 with $r_e$ = 1000 $\mu$m. While BC shifts the visible absorption to nearer the surface, a much greater portion of total absorption is in the visible spectrum. Even with large BC concentrations, visible absorption tends to occur deeper than NIR absorption. Most NIR absorption occurs in the top 1 mm of snow [*Brandt and Warren*, 1993; *Flanner and Zender*, 2005]. With sufficiently high BC concentrations, however, absorption shifts to higher in the snowpack, as can be seen by the slight downward trend in sub-2 cm absorption for $r_e$ = 50 $\mu$m and BC concentrations greater than 400 ng $g^{-1}$. The BC concentration of maximum sub-2 cm absorption depends on $r_e$ because of the visible depth-penetration dependence on $r_e$. If aerosol is more concentrated at the snow surface, however, because of dry deposition or accumulation of impurities near the snow surface during melt, total absorption shifts toward the surface. By influencing subsurface melt [*Koh and Jordan*, 1995], changes to the vertical distribution of heating can have important influence on snow climatology [*Flanner and Zender*, 2005].

### 3.2. GCM Experiments

[37] We conducted six GCM experiments with BC in snow, using configurations presented in Table 1, designated from here on as YYYY low, central, or high experiment, where YYYY is 1998 or 2001. To assess climate response and efficacy, we also completed paired control simulations for the central and high experiments (YYYY central and high control), identical to the experiments except without BC in snow. Forcing in the low experiments was insufficient to perturb climate. To help constrain efficacy, we also conducted experiment and control simulations with 10× 1998 BC and OC emission inventories (1998 10× experiment and control), with otherwise central model configurations (Table 1). Finally, to help discern the relative forcing contributions from FF, BF, and BB sources, we conducted experiments emitting only FF + BF and FF central estimate sources (FF + BF and FF experiments). All runs apply annually repeating emissions.

[38] The wide range of climate perturbation in these experiments required different spin-up periods for equilibrium. In the discussion that follows, we report results from the final 15 years of 16-year simulations (1998 and 2001 low, FF + BF, and FF experiment), 25-year simulations (1998 and 2001 central experiments and controls), and 35-year simulations (1998 and 2001 high experiments and controls). For the 1998 10× experiment and control, we analyze the final 20 years of 50-year simulations. The 95% confidence interval of linear trend in global mean 2-meter air temperature ($T_{2m}$) of these 15- and 20-year time series included zero for all experiments and controls except 2001 central and high experiments, which both had trends of +0.01°C $yr^{-1}$. Because the corresponding controls had no trend, it is possible we underestimated the climate response for these scenarios. Global mean top-of-model (TOM, about 3 mb pressure) radiative energy flux, averaged over the analysis periods, was within 1 W $m^{-2}$ of equilibrium for all model runs.

### 3.3. Measured and Modeled BC Concentrations in Snow

[39] Table 2 summarizes measurements of present-day BC in snowpack from all studies known to the authors. When mean values are not reported in the original literature, we report means of all published measurements from each location. Measurement techniques and uncertainties vary considerably between studies and are discussed to varying degrees in each reference. Most studies utilize optical or thermal/optical techniques, although *Slater et al.* [2002] applied an acid-base/thermal method. Table 2 also shows CAM/SNICAR predictions of BC concentrations in the surface snow layer. Data in the lower portion of the table show BC concentrations in precipitation, with model estimates derived from wet deposition and precipitation rates. When the measurements correspond to a particular time of year, we report model predictions from the same months. Otherwise, model results are annual mean estimates. Central estimates for 1998 and 2001 are reported with low-high range in parentheses. A log-log whisker plot of these data is shown in Figure 4. The center model point on this plot is the mean of 1998 and 2001 central experiments, and vertical error bar represents the greatest minimum-maximum range from both 1998 and 2001 low and high experiments. Global distributions of model annual mean BC concentrations in surface snow, averaged only when snow is present, are shown in Figure 5 for FF + BF and 1998 (FF + BF + BB) central estimates, plotted on a log scale.

[40] Figure 4 shows that central estimate BC/snow predictions capture the nearly 4 orders of magnitude range in observations with no apparent systematic bias. The correlation coefficient of the log of central model estimates and mean observations is 0.78. Furthermore, in nearly all cases, there is some overlap between the range of measurements and low-high model predictions.

**Table 2.** Comparison of Modeled and Measured BC in Snow, Sea-Ice, and Precipitation

| Site | Reference | Measurement Period | Measured BC[a], ng g$^{-1}$ | 1998 Model BC central (low-high) | 2001 Model BC central (low-high) |
|---|---|---|---|---|---|
| Summit, Greenland (72.6°N, 38.5°W) | *Slater et al.* [2002] | 1994–1996 | 14.6 (4.2–30.1) | 5.2 (1.7–64.1) | 3.5 (1.5–34.5) |
| | *Cachier* [1997] | 1991–1995 | 2.0–19.0[b] | | |
| | *Chylek et al.* [1995] | 1989–1990 | 2.0 (1.5–2.7) | | |
| | *Cachier and Pertuisol* [1994] | 1988–1989 | 1.0–4.0[b] | | |
| Camp Century, Gr. (77.2°N, 61.1°W) | *Chylek et al.* [1987] | ~1985 | 2.4 (2.1–2.6) | 13.3 (1.2–26.9) | 6.2 (0.9–19.6) |
| Dye 3, Greenland (65.2°N, 43.8°W) | *Clarke and Noone* [1985] | May 1983 | 6.4 (4.3–8.5) | 11.8 (3.6–131) | 8.2 (3.0–29.1) |
| Alert, N. Canada 83.5°N, 62.5°W) | *Clarke and Noone* [1985] | Nov.-Dec. 1983 | 56.9 (0–127) | 2.2 (0.9–5.9) | 2.5 (1.0–6.0) |
| Greenland Sea (79.8°N, 4.2°W) | *Clarke and Noone* [1985] | Jul. 1983 | 38.7 (5.4–75.5) | 23.9 (3.0–104) | 20.4 (3.5–93.9) |
| Spitzbergen (79°N, 12°E) | *Clarke and Noone* [1985] | May 1983 | 30.9 (6.7–52) | 12.7 (3.7–37.0) | 7.2 (4.6–34.4) |
| Barrow (71.3°N, 156.6°W) | *Clarke and Noone* [1985] | Apr. 1983, Mar. 1984 | 22.9 (7.3–60.4) | 9.7 (4.1–26.4) | 8.4 (3.2–25.4) |
| Abisko (68.3°N, 18.5°E) | *Clarke and Noone* [1985] | Mar.-Apr. 1984 | 33.0 (8.8–77) | 80.7 (15.3–332) | 96.4 (19.4–279) |
| Hurricane Hill (48.0°N, 123.5°W) | *Clarke and Noone* [1985] | Mar. 1984 | 14.7 (10.1–18.5) | 29.5 (7.1–101) | 35.2 (7.1–125) |
| Arctic Ocean (76°N, 165°E) | *Grenfell et al.* [2002] | Mar.-Apr. 1998 | 4.4 (1–9) | 8.4 (4.2–21.8) | 5.8 (2.4–16.7) |
| Cascades, Wash (~47°N, 121°W) | *Grenfell et al.* [1981] | Mar. 1980 | 22–59 | 36.8 (6.3–86.3) | 35.1 (6.7–85.9) |
| Halifax, Nova Scotia (45°N, 64°W) | *Chylek et al.* [1999] | Nov. 1995–Mar. 1996 | 11 (4.3–32) | 84.0 (22.0–244) | 84.9 (18.9–270) |
| French Alps (45.4°N, 5.3°E) | *Sergent et al.* [1993] | winters 1989–1991 | 161 (80–280) | 165 (50.5–226) | 136 (37.7–287) |
| | *Sergent et al.* [1998] | winters ~1992–1997 | 123 (34–247) | | |
| | *Fily et al.* [1997] | Apr. 1992 | 482 (235–826) | 394 (92.2–)[c] | 69.4 (32.7–498)[c] |
| | *Fily et al.* [1997] | Dec. 1992 | 115 (22–302) | 29.0 (37.4–349) | 43.5 (17.6–51.5) |
| West Texas/New Mexico (32°N, 106°W) | *Chylek et al.* [1987] | 1982–1985 | 10.6 (2.2–25.4) | 31.6 (8.4–89.6) | 15.5 (6.4–73.0) |
| Vostok (78.5°S, 106.9°E) | *Grenfell et al.* [1994] | Dec. 1990–Feb. 1991 | 0.6 | 1.08 (0.07–2.1) | 0.50 (0.07–1.8) |
| Siple Dome, Ant. (81.7°S, 148.8°W) | *Chylek et al.* [1987] | 1982–1985(?) | 2.5 (2.3–2.9) | 0.08 (0.04–0.68) | 0.09 (0.04–0.51) |
| South Pole (90°S) | *Warren and Clarke* [1990] | Jan.-Feb. 1986 | 0.23 (0.10–0.34) | 0.20 (0.07–1.23) | 0.21 (0.06–1.2) |
| | | *BC in Precipitation* | | | |
| Rural Michigan (45.5°, 84.7°W) | *Cadle and Dasch* [1988][d] | Dec.-Apr 1984–1985 | 72 (28–210) | 50 (22–108) | 46 (21–98) |
| Urban Michigan (42.5°N, 83°W) | *Dasch and Cadle* [1989][d] | Jan.-Apr 1984–1985 | 160 (17–5700) | 57 (26–132) | 53 (23–113) |
| Lithuania (55.5°N, 21°E) | *Armalis* [1999][e] | Dec. 1986–Jun. 1990 | 100 (8–530) | 61 (22–177) | 56 (20–179) |

[a]When mean values are not reported in the original literature, we report means of all published values from each location.
[b]As reported by *Slater et al.* [2002].
[c]Model results from March used in place of April; no March snow in 1998 high experiment.
[d]Snow precipitation.
[e]Snow + rain precipitation.

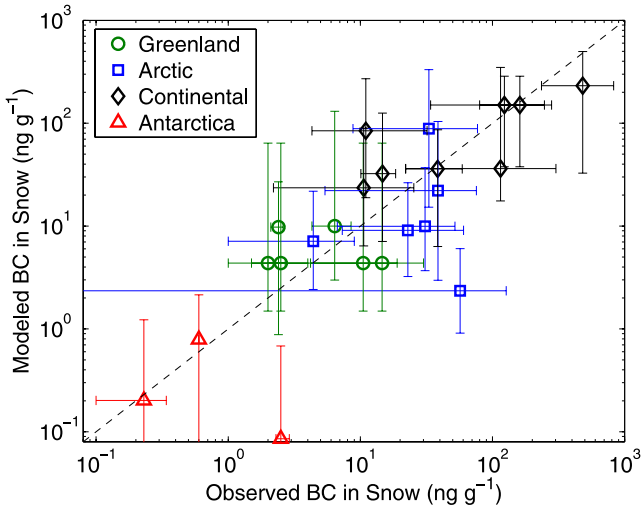


**Figure 4.** Model versus observed BC concentrations in near-surface snow for data from Table 2, grouped by region (precipitation measurements excluded). Model data are from the top 2 cm of snowpack. The center model point on this plot is the mean of 1998 and 2001 central experiments. The upper extent of the model error bar represents the maximum of 1998 and 2001 high experiments, whereas the lower extent is the minimum of both low experiments. The correlation coefficient of the log of these data is 0.78.

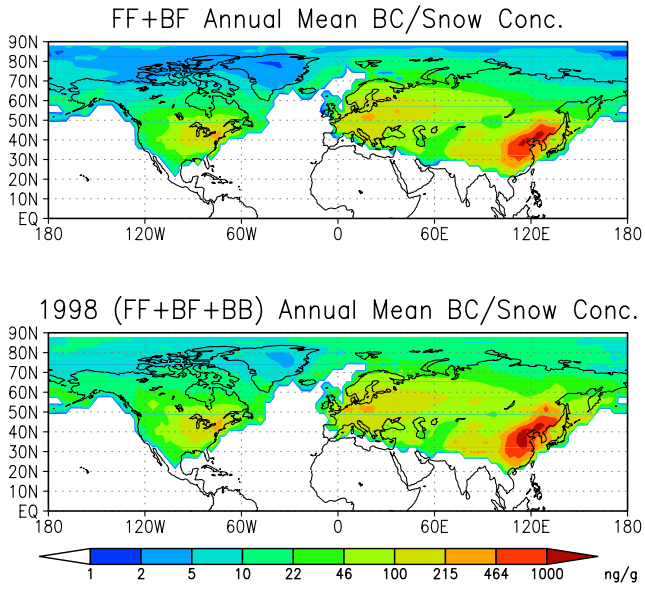


**Figure 5.** Annual mean predicted BC concentrations in snow (ng BC per g of ice) using central estimate (top) fossil fuel and biofuel sources only, and (bottom) fossil fuel, biofuel, and 1998 biomass burning emission sources.

**Table 3.** Summary of Model Experiment Results

| Model Scenario | $F_{s,snow}$[a], W m$^{-2}$ | Land frac.[b] of $F_{s,snow}$ | $F_{s,snow}$ LAND[c], W m$^{-2}$ | $F_{s,snow}$ ICE[d], W m$^{-2}$ | $\Delta T_{2m}$[e], °C | Efficacy[f] | $F_{t,atm}$[g], W m$^{-2}$ |
|---|---|---|---|---|---|---|---|
| 1998 low | +0.007 ± 8% | 0.73 | +0.08 | +0.04 | – | – | +0.07 ± 14% |
| 1998 central | +0.054 ± 7% | 0.82 | +0.60 | +0.23 | +0.15 ± 0.03 | $4.52^{+0.98}_{-0.97}$ | +0.37 ± 2% |
| 1998 high | +0.131 ± 6% | 0.83 | +1.56 | +0.79 | +0.23 ± 0.02 | $2.83^{+0.35}_{-0.34}$ | +1.31 ± 1% |
| 2001 low | +0.007 ± 9% | 0.74 | +0.07 | +0.04 | – | – | +0.05 ± 11% |
| 2001 central | +0.049 ± 7% | 0.83 | +0.55 | +0.20 | +0.10 ± 0.03 | $3.29^{+1.12}_{-1.11}$ | +0.28 ± 2% |
| 2001 high | +0.122 ± 6% | 0.83 | +1.42 | +0.75 | +0.16 ± 0.03 | $2.11^{+0.37}_{-0.37}$ | +1.09 ± 1% |
| FF + BF | +0.043 ± 5% | 0.85 | +0.48 | +0.15 | – | – | +0.19 ± 5% |
| FF | +0.033 ± 6% | 0.85 | +0.26 | +0.12 | – | – | +0.10 ± 4% |
| 1998 10× | +0.277 ± 3% | 0.77 | +2.90 | +1.11 | +0.54 ± 0.02 | $3.11^{+0.15}_{-0.14}$ | +4.96 ± 1% |

[a]Global annual mean of BC/snow instantaneous surface forcing.
[b]Fraction of $F_{s,snow}$ acting over land.
[c]$F_{s,snow}$ averaged spatially and temporally only over land snowpack.
[d]$F_{s,snow}$ averaged spatially and temporally only over snow on sea-ice.
[e]Equilibrium change in global annual mean $T_{2m}$ relative to control simulations without BC in snow.
[f]See equation (4).
[g]Global annual mean top-of-model (TOM) forcing from atmospheric BC + OC.

[41] Central model predictions are within the range of observations on Greenland and Antarctica, indicating reasonable model long-range BC transport. An exception is Siple Dome, where *Chylek et al.* [1987] reported measurements an order of magnitude greater than more recent Antarctic observations [*Warren and Clarke*, 1990; *Grenfell et al.*, 1994]. Measurements in Table 2 are not time resolved, except for *Slater et al.* [2002], who reported elemental carbon (EC, often considered synonymous with BC) concentrations with quarter-annual resolution, varying from 4 to 30 ng g$^{-1}$ over the course of two years. EC concentration spiked in the fall of 1994, although $^{14}$C analysis shows a predominantly fossil fuel-derived source. At Summit, monthly mean BC concentrations vary from 2 to 10 and from 7 to 330 ng g$^{-1}$ in our 1998 central and high estimate experiments, respectively, peaking in August and July.

[42] None of the measurements overlap our two years of emission scenarios. Because of interannual variability in biomass burning and trends in regional fossil fuel use, validity of this model-measurement comparison is therefore reduced. For example, our predictions are lower than four arctic measurements [*Clarke and Noone*, 1985] made in the early 1980s, when BC emissions from the former Soviet Union were much greater than today [*Novakov et al.*, 2003].

[43] Conversely, predictions exceed measurements at Abisko (Sweden), Hurricane Hill (Washington) [*Clarke and Noone*, 1985], and Halifax [*Chylek et al.*, 1999]. While Hurricane Hill may be representative of long-range transport because of prevailing westerlies, it is in the same model grid cell as Seattle and has a large local source. Measurements east of Seattle by *Grenfell et al.* [1981] show double the concentrations from Hurricane Hill, in accord with central model predictions. Halifax has a smaller, but still significant, local source. *Chylek et al.* [1999] specifically measured urban areas, however, so our model may have a high bias in this region. Low predictions are in range of measurements at Halifax and Abisko. In the French Alps near Grenoble, central model estimates agree well with those of *Sergent et al.* [1993], but are lower than those of *Fily et al.* [1997]. Central estimates of BC concentrations in precipitation are within range of measurements in rural Michigan [*Cadle and Dasch*, 1988] and Lithuania [*Armalis*, 1999], although they are lower than measurements made near Detroit [*Dasch and Cadle*, 1989].

[44] The largest predicted BC concentrations in snow are in northeast China (Figure 5), near strong industrial sources. There, concentrations in excess of 1000 ng g$^{-1}$ can lower snow albedo by more than 0.13. Annual mean concentrations in the eastern USA and Europe exceed 100 ng g$^{-1}$, enough to lower snow albedo by >0.03, depending on $r_e$. While fossil fuel-derived BC is the dominant source of midlatitude BC in snow, the effect of strong 1998 wildfires can be seen across the Arctic and Greenland (Figure 5). Annual mean BC concentrations in snow averaged over Greenland are 44% greater in 1998 than 2001. Comparing with the FF + BF simulation, we estimate that 43% and 24% of the annual mean BC in arctic snow (66.5–90°N) is from biomass sources in 1998 and 2001, respectively. During summer (June, July, and August), these BB source fractions rise to 60% and 36%.

[45] Summer atmospheric conditions favor enhanced wet and dry arctic BC deposition rates [*Stohl*, 2006], implying greater summer BC concentrations in snow regardless of temporal variability in emissions. *Koch and Hansen* [2005] predict that South Asia is the largest source of tropospheric arctic BC, but *Stohl* [2006] contests this and predicts that biomass sources dominate summer arctic BC using a mean 1980s burning inventory [*Lavoue et al.*, 2000]. *Stohl* [2006] also suggests that Siberian fires, and northern Eurasia sources in general, can reach the Arctic more easily than emissions from other regions of similar latitude. Future studies should use reanalysis winds to study the impact of individual fire events.

### 3.4. Global Mean Forcing and Response

[46] Table 3 lists for all experiments (from left to right) the global annual mean surface forcing from BC in snow ($F_{s,snow}$), the fraction of $F_{s,snow}$ acting over land (where the remaining fraction operates over sea-ice), $F_{s,snow}$ averaged temporally and spatially only over snow-covered land surface, $F_{s,snow}$ averaged only over sea-ice, the change in global annual mean $T_{2m}$ ($\Delta T_{2m}$) relative to control simulations without BC in snow, forcing "efficacy," and finally TOM forcings from atmospheric BC + OC ($F_{t,atm}$). Efficacy is defined as [*Hansen et al.*, 2005]:

$$E = \frac{\Delta T_s / F_a}{\Delta T_s(CO_2) / F_a(CO_2)} \quad (4)$$

where $F_a$ is the forcing at the tropopause after stratospheric adjustment [e.g., *Hansen et al.*, 1997] and $\Delta T_s$ is the change in global mean surface air temperature. The denominator is the response-to-forcing ratio from $CO_2$. *Hansen et al.* [2005] used forcing and temperature response from 1.5× preindustrial $CO_2$ levels. We apply CAM3 slab ocean model results from *Kiehl et al.* [2006], who report $F_a(CO_2)$ = 3.58 W m$^{-2}$ and equilibrium $\Delta T_s(CO_2)$ = 2.47°C from a doubling of $CO_2$ (355–710 ppm). In deriving $F_a$ from $F_{s,snow}$, we assume that instantaneous forcing at the tropopause ($F_i$) is $0.91F_{s,snow}$, and that $F_a$ is equal to $F_i$ (i.e., there is negligible immediate stratospheric radiative adjustment to the surface forcing). The first assumption is derived from numerous off-line experiments with SWNB [*Zender et al.*, 1997]. We examined the change in net solar energy at 132 mb relative to that at the surface ($F_i/F_s$) for slight reductions in visible surface albedo of a typical snow surface (initial visible and NIR albedos of 0.97 and 0.60). With zenith angle varying from 20° to 70°, cloud extinction optical depth $\tau_{cld}$ varying from 0 to 50, and visible albedo reduction varying from 0 to 0.10, the ratio $F_i/F_s$ varies only from 0.94 to 0.96. While $F_s$ is substantially reduced under cloudy skies, $F_i/F_s$ remains large and constant. However, absorbing aerosol significantly reduces $F_i/F_s$, particularly when it resides beneath a cloud, as multiple scattering between snow and cloud enhances absorption by the aerosol. Absorption optical depth $\tau_a$ = 0.05 ($\lambda$ = 550 nm) can reduce $F_i/F_s$ to 0.44. But assuming global mean $\tau_a$ = 0.0096 inferred from AERONET scaling of aerosol climatologies [*Sato et al.*, 2003; *Koch*, 2001], $\tau_{cld}$ = 5, and zenith angle of 60°, we estimate $F_i/F_s$ = 0.91, which we apply to derive efficacy. The ranges reported in Table 3 represent standard deviation in the annual mean time series. The reported range of $\Delta T_{2m}$ assumes unpaired pools (of global mean temperature from each year of equilibrium simulation) with equal variance. Efficacy standard error combines, in quadrature, standard deviations of $F_{s,snow}$ and $\Delta T_{2m}$. Support for our second assumption (that $F_a$ equals $F_i$) comes from *Hansen et al.* [2005], who report $F_a$ for BC/snow forcing within 2% of $F_i$.

[47] Table 3 shows that global BC/snow forcing is small relative to forcing from atmospheric BC + OC (columns 2 and 8 in Table 3). When $F_{s,snow}$ is averaged spatially and temporally only over snow, however, central estimates suggest that 0.55–0.60 additional W m$^{-2}$ are absorbed by snowpack on land and 0.20–0.23 W m$^{-2}$ by sea-ice because of the immediate presence of BC in snowpack. Our central estimates of $F_{s,snow}$ = +0.054 and +0.049 W m$^{-2}$ predict ~10% greater forcing in 1998 than 2001. Comparison with the FF + BF run suggests that about 20% of the total forcing can be attributed to biomass burning in 1998 and 12% in 2001. Estimates from the study by *Hansen and Nazarenko* [2004] of $F_a$ = +0.16 W m$^{-2}$ were downgraded to +0.05 W m$^2$ [*Hansen et al.*, 2005] (corrected result published in Appendix A.5 of *Hansen et al.* [2007]). The latter estimate is derived from spatially varying BC deposition, but without a detailed radiative transfer solution for snow with BC.

[48] An estimate of $F_a$ from FF + BF BC in snow and ice from *Jacobson* [2004b] is +0.06 W m$^{-2}$ (M. Jacobson, personal communication, 2006), greater than our estimate of +0.039 W m$^{-2}$ (0.91 × 0.043 W m$^{-2}$). *Jacobson* [2004b] treats BC in snow with a radiative transfer approximation, but prescribes spatially and temporally uniform snow grain size and an empirical fall speed for BC removal from snowpack. Atmospheric aerosol and cloud physical processes are highly sophisticated in *Jacobson* [2004b], however. Size-resolved BC and hydrometeors (including graupel) interact in clouds and precipitation through nucleation and coagulation, and both first and second aerosol/cloud indirect effects are treated. These processes enable prediction of more realistic size distribution and mixing state of BC deposited on snow. Because BC ages rapidly in our model relative to the transport time from source to remote snow surface, 87% of the BC deposited on snow is via wet deposition (providing a minimum estimate of the hydrophilic BC fraction in snow). This is less than the 98% BC wet deposition fraction on snow reported by *Jacobson* [2004b], but likely greater than *Koch and Hansen* [2005], who reported that dry deposition is responsible for the majority of BC landing on Greenland. Model differences could be due to several reasons, including more explicit treatment of size-resolved in-cloud scavenging processes by *Jacobson* [2004b], different dry deposition velocities, and different spatial pattern of emissions relative to model snow cover.

[49] While $F_{s,snow}$ is small globally, its efficacy is very large. Mean efficacy from the five experiment/control pairs in Table 3 is 3.17 (2.1–4.5). Because the temperature signal/noise ratio is small for realistic (central estimate) BC/snow forcing, the 1998 10× experiment and control provide a more constrained efficacy estimate. (More years of analysis also improve statistical constraint of the temperature response.) Tight agreement between 1998 10× efficacy and the mean of the other experiments is also encouraging. We caution, however, that efficacy does not necessarily scale linearly with forcing magnitude for a given agent (Figure 25 of *Hansen et al.* [2005]). Global mean $T_{2m}$ cooled several degrees before achieving steady state in both 1998 10× experiment and control runs because of extreme atmospheric aerosol optical depth, in spite of a positive TOM aerosol forcing.

[50] *Hansen et al.* [2005] reported similarly large BC/snow efficacy of 2.7 (corrected result in Appendix A.5 of *Hansen et al.* [2007]), the largest efficacy of all forcings studied. Conversely, mean efficacy of atmospheric BC (~0.69) is less than $CO_2$ [*Hansen et al.*, 2005]. Possible reasons for even greater BC/snow efficacy in our study include (1) greater albedo change sensitivity to temperature change in the Intergovernmental Panel on Climate Change (IPCC) AR4 NCAR model relative to the GISS model [*Qu and Hall*, 2006], (2) representation in our model of impurity accumulation near the surface during spring melt, which enhances the forcing precisely when it can have the largest impact on snowmelt and thus snow-albedo feedback, and (3) representation in our model of dynamic snow grain growth, which is enhanced by excess snowpack heating from BC. Better constraint on efficacy will require larger ensembles of GCM simulations with varying initial conditions and is beyond the scope of this study.

[51] Forcing from atmospheric BC + OC ($F_{t,atm}$) is about 5–6× greater than BC in snow (Table 3). However, if forcings are scaled by their respective efficacies, as *Hansen et al.* [2005] suggest, the resulting atmospheric BC + OC and BC/snow "effective" forcings are of similar magnitude.

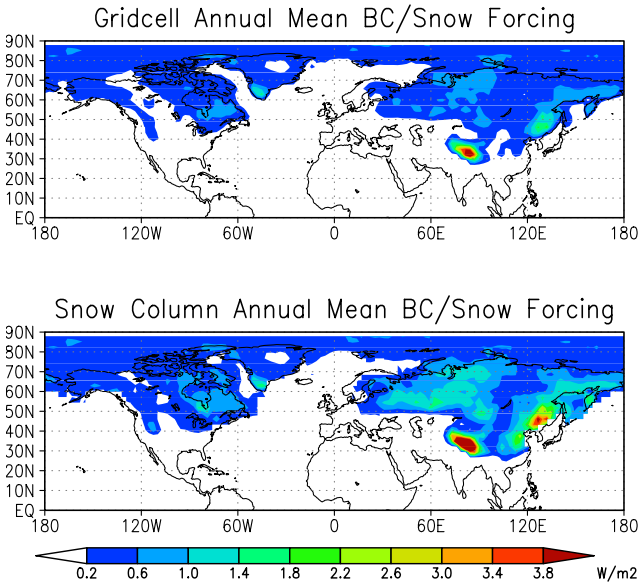


**Figure 6.** Central estimates of 1998 surface forcing (W $m^{-2}$) from BC in snow; (top) annual mean grid cell forcing, representing the true climate forcing; (bottom) forcing averaged spatially and temporally over only snow-covered surface, representing the mean increase in energy absorption by snowpack.

Much of the forcing from atmospheric BC is offset by OC, which is emitted simultaneously as BC in greater proportion, and which strongly scatters solar radiation. The net effect of atmospheric BC + OC forcing depends on aerosol optical properties, relative aerosol quantities, and reflectance of the underlying surface [e.g., *Ramanathan et al.*, 2001]. The OC/BC emission ratio is smaller in FF combustion than BB [e.g., *Bond et al.*, 2004]. Hence net radiative forcing from FF BC + OC is positive [e.g., *Jacobson*, 2001], whereas the sign of net forcing from BB BC + OC could be positive [e.g., *Hansen et al.*, 2005] or negative [e.g., *Myhre et al.*, 2003], depending especially on whether aerosol is lofted above clouds, where it is much more likely to have positive forcing. However, many other scattering aerosols are emitted in significant quantity from biomass burning, leading *Jacobson* [2004a] to suggest a global net surface cooling effect from all biomass burning aerosols. In our study, biomass burning contributes a much greater portion to $F_{t,atm}$ (49% and 32% in 1998 and 2001 central estimates, respectively) than to $F_{s,snow}$ (Table 3). Atmospheric aerosol forcing is not the focus of this study though, so we refrain from a detailed analysis.

### 3.5. Spatial/Temporal Climate Response Patterns

[52] The primary reason why BC/snow forcing is so efficacious is its ability to trigger snow-albedo feedback. Here we look at spatial and temporal distributions of forcing, snowmelt, albedo change, and temperature response to assess this feedback.

[53] Figure 6 depicts the Northern Hemisphere distribution of annual mean surface forcing from BC in snow for 1998. The top panel shows mean grid cell forcing, which depends on snow cover fraction. The bottom panel shows forcing averaged only over snow-covered surface within each grid cell, irrespective of SCF, and averaged only when snow is present. This metric describes the quantity of energy added specifically to snowpack, providing some insight into how local snowpack evolution may be affected. However, because model snow depth is very low in regions of low snow spatial coverage, and because forcing is reduced with shallow snowpack because of the radiative influence of the underlying ground, the snow-only forcing is significantly underestimated in unresolved mountainous terrain that should have deep snowpack. This deficiency can also be gleaned by noting very low snow-only forcing in the southernmost regions of model snow cover, where Figure 5 depicts large annual mean BC concentrations. The largest forcing is over the Tibetan Plateau (30–40°N, 80–100°E), averaging 1.5 W $m^{-2}$ over all land. Forcing over northeastern China and much of Eurasia becomes larger when considering snow-only forcing, as expected from large BC/snow concentrations (Figure 5) but modest snow cover fraction. During some spring months, snow-only forcing exceeds 10 and 20 W $m^{-2}$ over parts of eastern China and the Tibetan Plateau, respectively. Although BC mixing ratios and albedo reductions are greater in northeastern China, forcing is greater over the Tibetan Plateau because of greater ground-incident solar flux (because of closer proximity to the equator and less vegetation cover). More than 98% of the global forcing operates in the Northern Hemisphere.

[54] Maximum BC/snow forcing occurs with the combination of high BC concentrations in snow, surface-incident solar flux, and snow cover. This pattern is manifested in Figure 7, which shows Northern Hemisphere zonal, monthly mean surface forcing from BC in snow for 1998 and 2001 central estimates and derived estimates of the 1998 biomass burning contribution. The latitude of maximum forcing moves north as the spring progresses, following regions with large amounts of snow and incident sunlight. While BC emissions are consistent or stronger in fall than spring (1998 boreal fire intensity peaked in August and September), seasonal snowpack does not generally form before incident sunlight significantly diminishes, thus greatly reducing forcing during the accumulation phase. The 1998 arctic BC concentrations in snow peak in August, as opposed to July in 2001, attributable to boreal fires. But 80–90°N surface-incident solar flux drops to only 96 and 26 W $m^{-2}$ in August and September, reducing the radiative forcing potential. Thus April–June boreal fires have the greatest potential for strong BC/snow forcing. A second reason for greater forcing during the snowmelt phase is accumulation of impurities near the surface. This effect is controlled by the scavenging ratio (Table 1), which is largely unconstrained.

[55] The forcing space-time pattern in Figure 7 coincides closely with that of snowmelt onset. Thus BC/snow forcing, while generally small, is maximum precisely when it can have the greatest influence on snowmelt rate. Zonal-mean forcing is large at high latitudes, although BC concentrations are lower, because a greater portion of the surface is snow covered. Arctic forcing is 17% greater in 1998 than in 2001, and we attribute 35% of the total arctic forcing to biomass burning in 1998.

[56] Strong evidence for BC influence on snowmelt timing is seen in Figure 8, which shows change in zonal mean snowmelt rate (averaged over land only), resulting

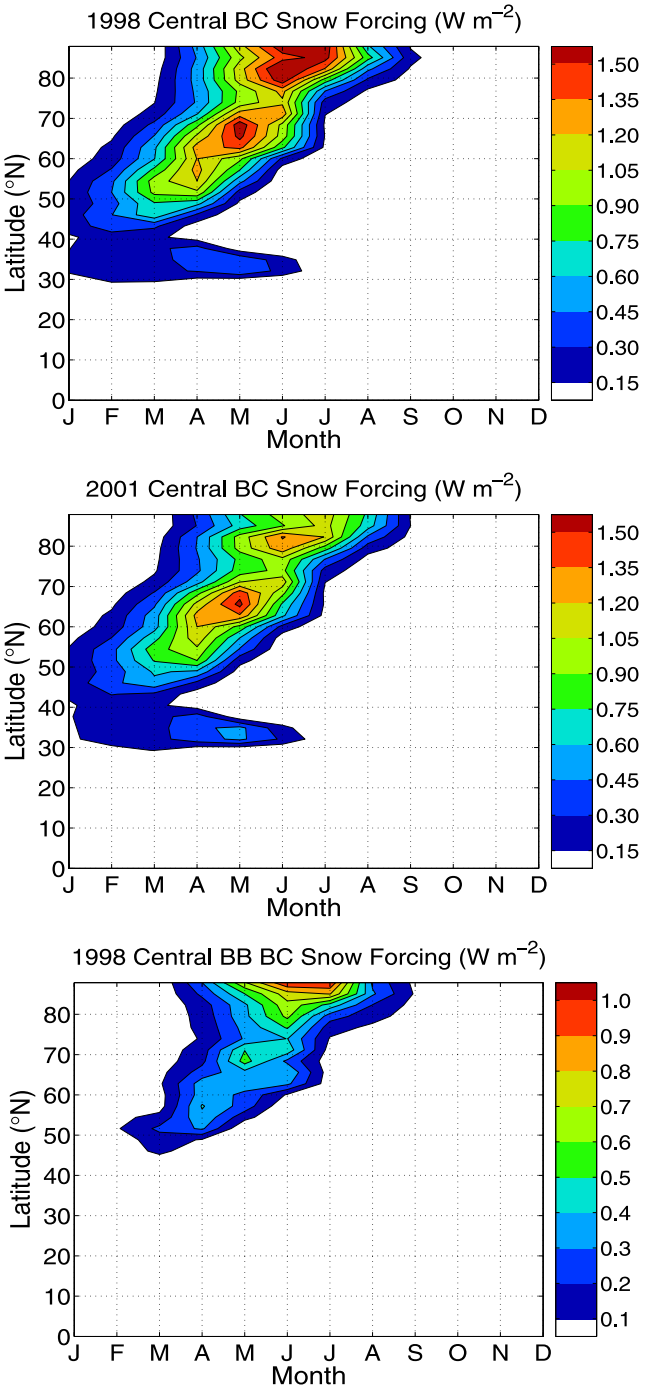


**Figure 7.** Zonal mean surface forcing from BC in snow as a function of month and latitude for (top) 1998 and (middle) 2001 central estimates, and (bottom) 1998 biomass burning only. The biomass burning forcing contribution is estimated as the difference between 1998 central (FF + BF + BB) and FF + BF only forcing.

from inclusion of BC in snow. Hatching shows statistically significant change at the 0.01 level. High-latitude melt rate clearly increases during the early snowmelt phase and decreases during the late melt phase, as there is less snow available. Quantified one way, zonal mean melt rate increases in the experiments by 8–54% in the month prior to maximum melt of the controls at latitudes north of 50°N. Area-weighted, this increase is 28% and 19% for 1998 and 2001, respectively. Figure 8 shows that statistically significant melt changes are more widespread in 1998 than 2001.

[57] Surface snowmelt on Greenland has been shown to increase the rate of ice sheet flow [*Zwally et al.*, 2002]. Summer mean melt rate averaged over Greenland is 3% and 13% greater in 1998 and 2001 central experiments than their respective controls, but these changes are not significant at the 0.05 level. Summer $T_{2m}$ warming over Greenland is 0.44°C in both central experiments. Corresponding warming in both 1998 and 2001 high experiments is 1.15°C, and melt rate changes are both significant at the 0.05 level. Central and high estimates of BC in Antarctic snow are too low to have significant influence on snow albedo, but we wonder if strong Australian wildfires could have a noticeable effect.

[58] Along with snowmelt changes are highly significant reductions in zonal mean surface albedo. Figure 9 shows these changes, averaged over land and ocean, with hatching

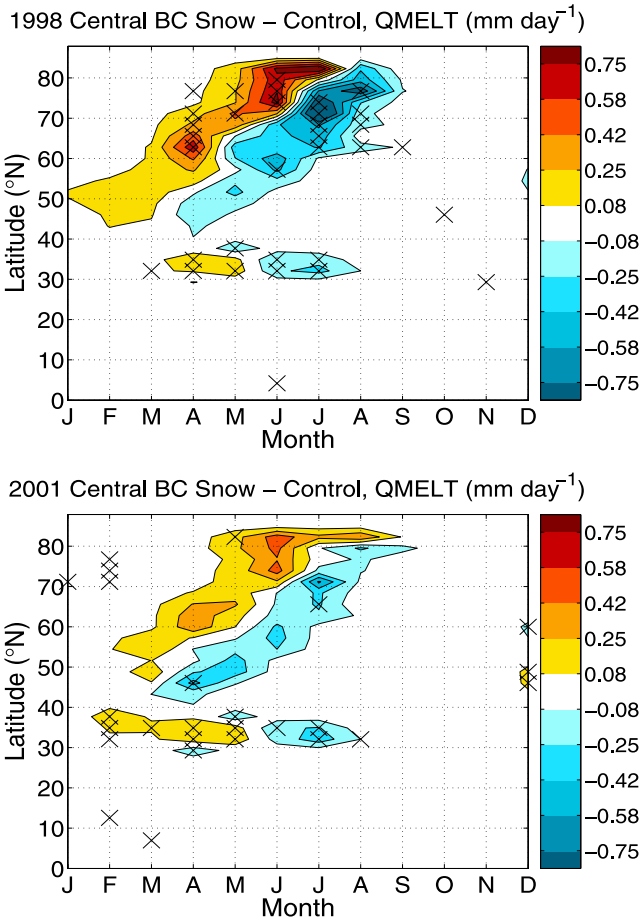


**Figure 8.** Difference in zonal monthly mean land snowmelt rate between central experiments and their respective controls. Experiment and control are identical except that BC only affects snow reflectance and heating in the experiment. Hatching shows statistically significant change at the 0.01 level.

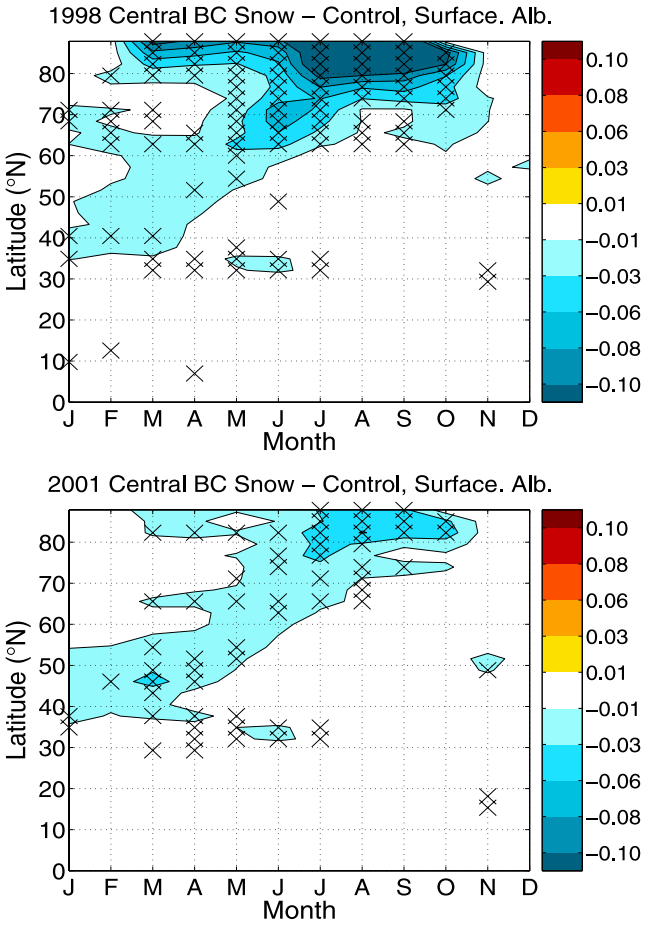


**Figure 9.** Difference in zonal monthly mean surface albedo between central BC/snow experiments and their respective controls. Hatching shows statistically significant change at the 0.01 level.

again at 0.01 significance. Annual mean albedo (weighted by surface insolation) of all arctic surface is reduced by 0.047 and 0.017 in 1998 and 2001 central experiments, respectively. The late-summer (August-September) 0.10–0.18 reduction in 80–90°N 1998 albedo happens because summer snow depth on sea-ice is reduced by 72%, exposing the darker bare sea-ice. This large reduction follows the 1.5 W $m^{-2}$ June-July BC/snow forcing (Figure 7).

[59] Observations spanning 1954–1991 from Soviet drifting stations indicate that snow on top of perennial sea-ice is generally nearly gone by July or August [*Warren et al.*, 1999]. Surface Heat Budget of the Arctic (SHEBA) observations from 1998 show snow ablation by early July [*Perovich et al.*, 2002], whereas model snow depth reaches August minimums of 29 and 13 cm in 1998 and 2001 central control simulations, and 5 and 11 cm in 1998 and 2001 central experiments, respectively. These observations indicate a model tendency of excessive snow cover on late-summer sea-ice. Perhaps encouragingly, the inclusion of BC in snow reduces model snow depth.

[60] Excess snowpack heating and climate feedback in the model also appear to accelerate snow grain growth, which darkens the snow itself and enhances the perturbation from BC (Figure 3). The increase in 80–90°N June and July $r_e$ relative to 1998 central control is 289 $\mu$m. The forcing responsible for this feedback is largely from biomass burning and is clearly damped in the 2001 central experiment (Figure 7), where 80–90°N June and July $r_e$ is only 52 $\mu$m greater than 2001 central control, summer snow depth on sea-ice reduced by only 13%, and late-summer albedo reduced by 0.05. Note that these results are sensitive to the CSIM snow height/SCF relationship [*Briegleb et al.*, 2004], which determines the proportion of exposed bare sea-ice. Slight changes to snow depths less than 10 cm have large impact on SCF and therefore albedo. In spite of large albedo reduction, sea-ice area changes are small. July–September mean arctic (66.5–90°N) sea-ice coverage is reduced by 3% and 1% in these two experiments relative to their respective control simulations.

[61] Finally, Figure 10 shows significant surface air warming from BC in snow, especially from 60 to 90°N during June-November, 1998. Annual mean $T_{2m}$ warming averaged over the arctic is +1.61 and +0.50°C for 1998 and 2001. The late-summer polar warming pattern in 1998 is logically coupled with the forcing and albedo change patterns described above. The 1998 winter and spring warming

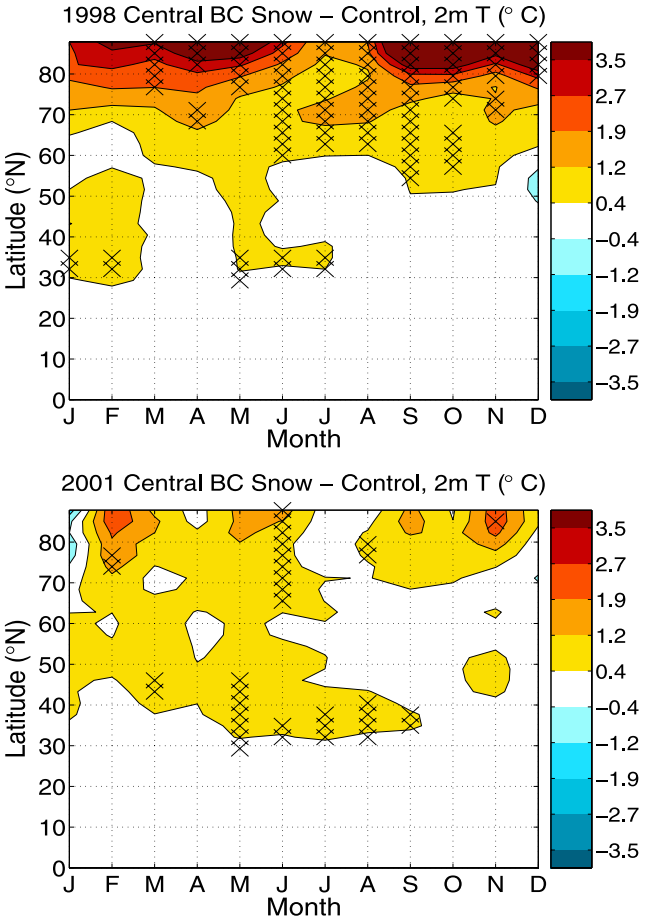


**Figure 10.** Difference in zonal monthly mean 2-meter air temperature between central BC/snow experiments and their respective controls. Hatching shows statistically significant change at the 0.01 level.

**Table 4.** Estimated Range of Change in Global Mean BC/Snow Radiative Forcing ($F_{s,snow}$), Represented as a Scalar, Resulting From Variation of Individual Factors[a]

| | Low | High |
|---|---|---|
| BC Emissions | 0.54 | 2.00 |
| Snow Aging | 0.58 | 1.58 |
| Melt Scavenging | 0.69 | 1.08 |
| Optical Properties | 0.88 | 1.12 |
| Snow Cover Fraction | 0.83 | 1.08 |

[a]The range is relative to 1998 central estimates, using low and high estimates of each factor in Table 1.

may be a consequence of thermal inertia from fall warming or could be dynamical in nature. We note that our 1998 central experiment showed the highest efficacy of all experiments, so we urge caution in assuming that the large responses discussed are due entirely to biomass burning emissions, which cause only a modest increase in forcing (Figure 7c).

[62] These changes provide evidence that significant snow-albedo feedback occurs from BC in snow, despite its small forcing. Reasons why BC and other aerosols can provoke disproportionately large responses include their ability to warm snow, either directly melting it or priming it for earlier melt, enhanced snow grain metamorphism, which darkens the snow itself and increases the radiative perturbation by impurities, and amassing of impurities at the surface during melt. Changes in the timing of snow ablation, however, have the greatest influence on the surface energy balance because of the huge contrast in surface reflectance between snow and most other surfaces. Hence the subtler effects of snow impurities come into play when they combine to influence snowmelt timing, as they apparently do in both 1998 and 2001 central experiments.

### 3.6. Individual Uncertainties

[63] Finally, we examine the influence, to first order, that each of the five uncertainties discussed in section 2 have individually on global BC/snow forcing. This offers insight into the relative importance of constraining uncertainty in each factor.

[64] To derive estimates of variability in global annual mean $F_{s,snow}$, we performed the following experiments: For the role of BC emission scenarios, we conducted two 6-year simulations using 1998 central configuration (Table 1), but with low and high emissions estimates. For optical properties, we conducted off-line 470-band SNICAR experiments, estimating hypothetical forcing assuming less absorptive and more absorptive BC, given annual mean BC concentration and $r_e$ at each grid cell of the 1998 central experiment. For snow aging, we also used off-line SNICAR to estimate forcing at each grid cell, assuming annual mean BC concentration from the 1998 central experiment, but using the corresponding annual mean $r_e$ from the 1998 low and high experiments, representing slow and rapid aging. (If a grid cell contained snow in the central experiment, but not in the high or low, we assumed the global mean high or low $r_e$). For the role of meltwater scavenging, we conducted another pair of 6-year CAM3 experiments with 1998 central configuration, but with meltwater scavenging factor ranging by 2 orders of magnitude (Table 1). Finally, we assess the role of SCF by scaling the BC/snow forcing at each grid cell of monthly output according to hypothetical SCF (calculated from snow depth), using the high and low representations discussed in section 2. Note that it would be more appropriate to estimate optical property and aging uncertainty at monthly resolution, as with SCF, but this would require an excessive number of off-line SNICAR runs.

[65] The range in mean $F_{s,snow}$ estimated with these approaches is shown in Table 4. Uncertainty in emissions has the largest bearing on BC/snow forcing, closely followed by snow aging. The low-high range of FF + BF emissions from *Bond et al.* [2004] is greater than the range we derived for BB emissions (Table 1). Some of this difference is because we derive uncertainty using an observational inversion constraint, whereas uncertainty from *Bond et al.* [2004] is derived from compounding forward uncertainties. Global mean snow $r_e$ varied from 91 to 812 $\mu$m between 1998 low and high experiments. While our choice of scaling snow aging by a factor of 2 was purely subjective, there are no observations of all relevant parameters required to constrain aging processes [*Flanner and Zender*, 2006]. Uncertainty in scavenging factor can significantly decrease the global forcing estimate, but can raise it only slightly. This happens because scavenging, even for hydrophilic impurities, is relatively inefficient in the central estimates. Thus decreasing the scavenging ratio increases the forcing only minimally in the high experiment, as impurities tend to reside near the surface during melt in the central experiment. Increasing the scavenging efficiency, however, significantly lowers the global forcing estimates, as impurities efficiently flush through the snowpack during the melt phase. *Grenfell et al.* [2002] reported relatively uniform vertical profiles of BC in the snow on sea-ice during the SHEBA campaign in late March and April 1998. More observations of BC profiles during the melt phase will help constrain scavenging ratios. Additional off-line SNICAR experiments showed that the range of effect of varying BC optical properties was relatively insensitive to snow grain size, in spite of the sensitivity of forcing to grain size (Figure 3), but the range narrowed slightly with increasing BC concentrations. Finally, the range of effect of SCF representation is small but slightly asymmetrical. This can be explained by the probability density function of snow depth where and when BC forcing operates. Snow depths greater than 20 predict SCF close to 1 with both central and high estimates, but much lower SCF with low estimates.

## 4. Conclusions

[66] We incorporate our SNICAR model into the NCAR CAM3 GCM to improve quantification of present-day forcing, climate response, and associated uncertainties from black carbon (BC) in snow. This is the first global climate study which treats coupled snow aerosol heating and snow aging. We assemble model scenarios which bound the plausible range of present-day BC/snow forcing using combinations of BC emissions, BC optical properties, snow aging, meltwater scavenging of BC, and snow cover fraction. We estimate global annual mean BC/snow surface radiative forcings from all BC sources of +0.054 (0.007–0.13) and +0.049 (0.007–0.12) W m$^{-2}$ during strong (1998) and weak (2001) boreal fire years, respectively. The forcing contri-

butions from only fossil fuel + biofuel and only fossil fuel sources are +0.043 and +0.033 W $m^{-2}$, respectively. Central estimate predictions of BC concentrations in snow capture the nearly 4 orders of magnitude range in observations with no apparent systematic bias, lending some confidence to our central forcing estimates. However, uncertainty in BC emissions and snow aging can individually account for a nearly twofold range in forward-modeled global forcing. Uncertainty arising from the other factors is of order 20%.

[67] Global annual mean equilibrium warming resulting from the inclusion of BC in snow is 0.15 and 0.10°C for 1998 and 2001 central experiments, respectively. Annual arctic (66.5–90°N) warming, however, is 1.61 and 0.50°C. Arctic annual mean surface albedo for these two experiments is reduced by 0.047 and 0.017, relative to their control simulations without BC in snow. The 1998 and 2001 land snowmelt rates north of 50°N are 28% and 19% greater in the month preceding maximum melt of control simulations. These statistically significant climate signals all indicate that snow-albedo feedback is triggered by present-day BC/snow forcing. Greater climate response in 1998 might be attributable to strong boreal fires, which increase arctic BC/snow forcing by 17% relative to 2001. Climate response in our 1998 central experiment was unusually strong, however, and more simulations are needed to test this hypothesis. The 1998 boreal fire strength peaked in August and September, whereas fires occurring in April–June have the greatest BC/snow forcing potential because of strong high-latitude insolation and large snow areal coverage. Even in the strong boreal fire year, we attribute 80% of the global BC/snow forcing to fossil fuel and biofuel sources.

[68] Mean efficacy [*Hansen et al.*, 2005] of our five experiments is 3.17 (2.1–4.5). This mean closely matches efficacy obtained from a long experiment with 10× present-day BC emissions, likely providing a more realistic efficacy estimate because of large temperature response relative to natural variability. BC in snowpack can provoke disproportionately large springtime climate response because the forcing tends to coincide with the onset of snowmelt, thus triggering more rapid snow ablation and snow-albedo feedback. The model and methods we develop here could be applied to study snow forcing by other aerosols, including mineral dust, volcanic ash, brown carbon, and marine sediment in sea-ice [*Light et al.*, 1998]. Sparseness of snow impurity measurements and uncertainty in snow effective radius variability suggest that more ground measurements need to be made and remote-sensing techniques refined to constrain understanding of this phenomenon on a global scale.

[69] **Acknowledgments.** We thank Steve Warren for insightful comments after reviewing our manuscript and providing the spectral albedo measurements for Figure 2. We also thank two anonymous reviewers for comments. We thank Tami Bond for providing advice and recent manuscripts on black carbon optical properties, Prasad Kasibhatla for providing carbon monoxide inversion factors, M. Andreae for providing updated fire emission factors, Tom Painter for the opportunity to observe and measure, first-hand, snow-impurity effects, and Dani Bundy and Mariana Vertenstein for advice on CAM/SNICAR coupling. Funding for this work was provided by NSF/NCAR SGER ATM-0503148 and NASA Earth System Science Fellowship NNG05GP30H. Computations are supported by Earth System Modeling Facility NSF ATM-0321380.

## References

Andrea, M. O., and A. Gelencser (2006), Black carbon or brown carbon? The nature of light-absorbing carbonaceous aerosols, *Atmos. Chem. Phys.*, *6*, 3131–3148.

Andreae, M. O., and P. Merlet (2001), Emission of trace gases and aerosols from biomass burning, *Glob. Biogeochem. Cycles*, *15*(4), 955–966.

Armalis, S. (1999), Wet deposition of elemental carbon in Lithuania, *Sci. Total Environ.*, *239*, 89–93.

Bond, T. C. (2001), Spectral dependence of visible light absorption by carbonaceous particles emitted from coal combustion, *Geophys. Res. Lett.*, *28*(21), 4075–4078.

Bond, T. C., and R. W. Bergstrom (2006), Light absorption by carbonaceous particles: An investigative review, *Aerosol Sci. Technol.*, *40*(1), 27–67, doi:10.1080/02786820500421521.

Bond, T. C., D. G. Streets, K. F. Yarber, S. M. Nelson, J.-H. Woo, and Z. Klimont (2004), A technology-based global inventory of black and organic carbon emissions from combustion, *J. Geophys. Res.*, *109*, D14203, doi:10.1029/2003JD003697.

Bond, T. C., G. Habib, and R. W. Bergstrom (2006), Limitations in the enhancement of visible light absorption due to mixing state, *J. Geophys. Res.*, *111*, D20211, doi:10.1029/2006JD007315.

Brandt, R. E., and S. G. Warren (1993), Solar-heating rates and temperature profiles in Antarctic snow and ice, *J. Glaciol.*, *39*(131), 99–110.

Briegleb, B. P. (1992), Delta-Eddington approximation for solar radiation in the NCAR Community Climate Model, *J. Geophys. Res.*, *97*(D7), 7603–7612.

Briegleb, B. P., C. M. Bitz, E. C. Hunke, W. H. Lipscomb, M. M. Holland J. L. Schramm, and R. E. Moritz (2004), Scientific description of the sea ice component in the Community Climate System Model, version three, *Tech. Rep. NCAR TN–463 + STR*, National Center for Atmospheric Research.

Brun, E. (1989), Investigation of wet-snow metamorphism in respect of liquid-water content, *Ann. Glaciol.*, *13*, 22–26.

Budyko, M. I. (1969), The effects of solar radiation on the climate of the earth, *Tellus*, *21*, 611–619.

Cachier, H. (1997), Particulate and dissolved carbon in air and snow at the Summit site, in *Transfer of Aerosols and Gases to Greenland Snow and Ice: Final Technical Report, Cedex, France*, pp. 21–27.

Cachier, H., and M. H. Pertuisol (1994), Particulate carbon in Arctic ice, *Anal. Mag.*, *22*, M34–M37.

Cadle, S. H., and J. M. Dasch (1988), Wintertime concentrations and sinks of atmospheric particulate carbon at a rural location in northern Michigan, *Atmos. Environ.*, *22*(7), 1373–1381.

Chang, H., and T. T. Charalampopoulos (1990), Determination of the wavelength dependence of refractive indices of flame soot, *Proc. R. Soc. London, Ser. A*, *430*(1880), 577–591.

Chylek, P., V. Srivastava, L. Cahenzli, R. G. Pinnick, R. L. Dod, and T. Novakov (1987), Aerosol and graphitic carbon content of snow, *J. Geophys. Res.*, *92*(D8), 9801–9809.

Chylek, P., B. Johnson, and P. A. Damiano (1995), Biomass burning record and black carbon in the GISP2 Ice Core, *Geophys. Res. Lett.*, *22*(2), 89–92.

Chylek, P., L. Kou, B. Johnson, F. Boudala, and G. Lesins (1999), Black carbon concentrations in precipitation and near surface air in and near Halifax, Nova Scotia, *Atmos. Environ.*, *33*, 2269–2277.

Clarke, A., and K. Noone (1985), Soot in the Arctic: A cause for perturbation in radiative transfer, *J. Geophys. Res.*, *19*(12), 2045–2053.

Collins, W. D. (2001), Parameterization of generalized cloud overlap for radiative calculations in general circulation models, *J. Atmos. Sci.*, *58*, 3224–3242.

Collins, W. D., P. J. Rasch, B. E. Eaton, D. W. Fillmore, and J. T. Kiehl (2002), Simulation of aerosol distributions and radiative forcing for INDOEX: Regional climate impacts, *J. Geophys. Res.*, *107*(D19), 8028, doi:10.1029/2000JD000032.

Collins, W. D., P. J. Rasch, B. A. Boville, J. J. Hack, J. R. McCaa, D. L. Williamson, J. T. Kiehl, and B. Briegleb (2004), Description of the NCAR Community Atmosphere Model (CAM 3.0), *Tech. Rep. NCAR TN–464+STR*, National Center for Atmospheric Research.

Conway, H., A. Gades, and C. F. Raymond (1996), Albedo of dirty snow during conditions of melt, *Water Resour. Res.*, *32*(6), 1713–1718.

Cooke, W. F., C. Liousse, and H. Cachier (1999), Construction of a 1 × 1 fossil fuel emission data set for carbonaceous aerosol and implementation and radiative impact in the ECHAM4 model, *J. Geophys. Res.*, *104*(D18), 22,137–22,162.

Dasch, J. M., and S. H. Cadle (1989), Atmospheric carbon particles in the Detroit urban area: Wintertime sources and sinks, *Aerosol Sci. Technol.*, *10*, 236–248.

Ebert, E. E., and J. A. Curry (1992), A parameterization of ice cloud optical properties for climate models, *J. Geophys. Res.*, *97*(D4), 3831–3836.

Fily, M., B. Bourdelles, J. P. Dedieu, and C. Sergent (1997), Comparison of in situ and Landsat Thematic Mapper derived snow grain characteristics in the Alps, *Remote Sens. Environ.*, *59*, 452–460.

Flanner, M. G., and C. S. Zender (2005), Snowpack radiative heating: Influence on Tibetan Plateau climate, *Geophys. Res. Lett.*, *32*, L06501, doi:10.1029/2004GL022076.

Flanner, M. G., and C. S. Zender (2006), Linking snowpack microphysics and albedo evolution, *J. Geophys. Res.*, *111*, D12208, doi:10.1029/2005JD006834.

Ganguly, D., A. Jayaraman, H. Gadhavi, and T. A. Rajesh (2005), Features in wavelength dependence of aerosol absorption observed over central India, *Geophys. Res. Lett.*, *32*, L13821, doi:10.1029/2005GL023023.

Grenfell, T. C., and S. G. Warren (1999), Representation of a nonspherical ice particle by a collection of independent spheres for scattering and absorption of radiation, *J. Geophys. Res.*, *104*(D24), 31,697–31,709.

Grenfell, T. C., D. K. Perovich, and J. A. Ogren (1981), Spectral albedos of an alpine snowpack, *Cold Reg. Sci. Technol.*, *4*, 121–127.

Grenfell, T., S. Warren, and P. Mullen (1994), Reflection of solar radiation by the Antarctic snow surface at ultraviolet, visible, and near-infrared wavelengths, *J. Geophys. Res.*, *99*(D9), 18,669–18,684.

Grenfell, T., B. Light, and M. Sturm (2002), Spatial distribution and radiative effects of soot in the snow and sea ice during the SHEBA experiment, *J. Geophys. Res.*, *107*(C10), 8032, doi:10.1029/2000JC000414.

Grenfell, T. C., S. P. Neshyba, and S. G. Warren (2005), Representation of a nonspherical ice particle by a collection of independent spheres for scattering and absorption of radiation: 3. Hollow columns and plates, *J. Geophys. Res.*, *110*, D17203, doi:10.1029/2005JD005811.

Hansen, J., and L. Nazarenko (2004), Soot climate forcing via snow and ice albedos, *Proc. Natl. Acad. Sci.*, *101*(2), 423–428.

Hansen, J., M. Sato, and R. Ruedy (1997), Radiative forcing and climate response, *J. Geophys. Res.*, *102*, 6831–6864.

Hansen, J., et al. (2005), Efficacy of climate forcings, *J. Geophys. Res.*, *110*, D18104, doi:10.1029/2005JD005776.

Hansen, J., et al. (2007), Climate simulations for 1880–2003 with GISS ModelE, *Clim. Dyn.*, in press.

Hess, M., P. Koepke, and I. Schult (1998), Optical properties of aerosols and clouds: The software package OPAC, *Bull. Am. Meteorol. Soc.*, *79*(5), 831–844.

Hoffer, A., A. Gelencser, P. Guyon, G. Kiss, O. Schmid, G. Frank, P. Artaxo, and M. O. Andreae (2006), Optical properties of humic-like substances (HULIS) in biomass-burning aerosols, *Atmos. Chem. Phys.*, *6*, 3563–3570.

Jacobson, M. (2001), Strong radiative heating due to the mixing state of black carbon, *Nature*, *409*, 695–697.

Jacobson, M. Z. (2004a), The short-term cooling but long-term global warming due to biomass burning, *J. Clim.*, *17*, 2909–2926.

Jacobson, M. Z. (2004b), Climate response of fossil fuel and biofuel soot, accounting for soot's feedback to snow and sea ice albedo and emissivity, *J. Geophys. Res.*, *109*(D21201), doi:10.1029/2004JD004945.

Jordan, R. (1991), A one-dimensional temperature model for a snow cover: Technical documentation for SNTHERM 89., *Tech. Rep. Special Report 91-16*, U.S. Army Cold Regions Research and Engineering Laboratory.

Joseph, J. H., W. J. Wiscombe, and J. A. Weinman (1976), The delta-Eddington approximation for radiative flux transfer, *J. Atmos. Sci.*, *33*, 2452–2459.

Kiehl, J. T., C. A. Shields, J. J. Hack, and W. D. Collins (2006), The climate sensitivity of the Community Climate System Model: CCSM3, *J. Clim.*, *19*, 2854–2596.

Kirchstetter, T. W., T. Novakov, and P. V. Hobbs (2004), Evidence that the spectral dependence of light absorption by aerosols is affected by organic carbon, *J. Geophys. Res.*, *109*, D21208, doi:10.1029/2004JD004999.

Koch, D. (2001), Transport and direct radiative forcing of carbonaceous and sulfate aerosols in the GISS GCM, *J. Geophys. Res.*, *106*(D17), 20,311–20,332.

Koch, D., and J. Hansen (2005), Distant origins of Arctic black carbon: A Goddard Institute for Space Studies ModelE experiment, *J. Geophys. Res.*, *110*, D04204, doi:10.1029/2004JD005296.

Koh, G., and R. Jordan (1995), Sub-surface melting in a seasonal snow cover, *J. Glaciol.*, *41*, 474–482.

Lavoue, D., C. Liousse, H. Cachier, B. J. Stocks, and J. G. Goldammer (2000), Modeling of carbonaceous particles emitted by boreal and temperate wildfires at northern latitudes, *J. Geophys. Res.*, *105*(D22), 26,871–26,890.

Light, B., H. Eicken, G. A. Maykut, and T. C. Grenfell (1998), The effect of included particulates on the spectral albedo of sea ice, *J. Geophys. Res.*, *103*(C12), 27,739–27,752.

Myhre, G., T. K. Berntsen, J. M. Haywood, J. K. Sundet, B. N. Holben, M. Johnsrud, and F. Stordal (2003), Modeling the solar radiative impact of aerosols from biomass burning during the Southern African Regional Science Initiative (SAFARI-2000) experiment, *J. Geophys. Res.*, *108*(D13), 8501, doi:10.1029/2002JD002313.

Neshyba, S., T. Grenfell, and S. Warren (2003), Representation of a nonspherical ice particle by a collection of independent spheres for scattering and absorption of radiation: 2. Hexagonal columns and plates, *J. Geophys. Res.*, *108*(D15), 4448, doi:10.1029/2002JD003302.

Novakov, T., V. Ramanathan, J. E. Hansen, T. W. Kirchstetter, M. Sato, J. E. Sinton, and J. A. Sathaye (2003), Large historical changes of fossil-fuel black carbon aerosols, *Geophys. Res. Lett.*, *30*(6), 1324, doi:10.1029/2002GL016345.

Oleson, K. W., et al. (2004), Technical description of the Community Land Model (CLM), *Tech. Rep. NCAR TN-461+STR*, National Center for Atmospheric Research.

Painter, T. H., J. Dozier, D. A. Roberts, R. E. Davis, and R. O. Greene (2003), Retrieval of subpixel snow-covered area and grain size from imaging spectrometer data, *Remote. Sens. Environ.*, *85*, 64–77.

Perovich, D. K., T. C. Grenfell, B. Light, and P. V. Hobbs (2002), Seasonal evolution of the albedo of multiyear Arctic sea ice, *J. Geophys. Res.*, *107*(C10), 8044, doi:10.1029/2000JC000438.

Qu, X., and A. Hall (2006), Assessing snow albedo feedback in simulated climate change, *J. Clim.*, *19*, 2617–2630.

Ramanathan, V., et al. (2001), Indian Ocean Experiment: An integrated analysis of the climate forcing and effects of the great Indo-Asian haze, *J. Geophys. Res.*, *106*(D22), 28,371–28,398.

Rasch, P. J., and J. E. Kristjánsson (1998), A comparison of the CCM3 climate model using diagnosed and predicted condensate parameterizations, *J. Clim.*, *11*, 1587–1614.

Rasch, P. J., W. D. Collins, and B. E. Eaton (2001), Understanding the Indian Ocean Experiment (INDOEX) aerosol distributions with an aerosol assimilation, *J. Geophys. Res.*, *106*(D7), 7337–7355.

Rasch, P. J., M. Fromm, O. Torres, D. J. Diner, R. Kahn, and J. Martonchik (2005), An exploratory study of the impact of pyro-cumulonimbus injections of aerosol on the upper troposphere and lower stratosphere climate during Northern Hemisphere summer, *Eos Trans. AGU*, *86*(52), Fall Meet. Suppl., Abstract A22B-01.

Romanov, P., and D. Tarpley (2004), Estimation of snow depth over open prairie environments using GOES imager observations, *Hydrol. Processes*, *18*, 1073–1087, doi:10.1002/hyp.5508.

Sato, M., J. Hansen, D. Koch, A. Lacis, R. Reudy, O. Dubovik, B. Holben, M. Chin, and T. Novakov (2003), Global atmospheric black carbon inferred from AERONET, *Proc. Natl. Acad. Sci.*, *100*, 6319–6324.

Schnaiter, M., H. Horvath, O. Möhler, K.-H. Naumann, H. Saathoff, and O. W. Schöck (2003), UV-VIS-NIR spectral optical properties of soot and soot-containing aerosols, *J. Aerosol Sci.*, *34*(10), 1421–1444.

Sergent, C., E. Pougatch, and M. Sudul (1993), Experimental investigation of optical snow properties, *Ann. Glaciol.*, *17*, 281–287.

Sergent, C., C. Leroux, E. Pougatch, and F. Guirado (1998), Hemispherical-directional reflectance measurements of natural snow: Comparison with adding-doubling modeling, *Ann. Glaciol. Soc.*, *26*, 59–63.

Slater, J. F., L. A. Currie, J. E. Dibb, and J. B. A. Benner (2002), Distinguishing the relative contribution of fossil fuel and biomass combustion aerosols deposited at Summit, Greenland through isotopic and molecular characterization of insoluble carbon, *Atmos. Environ.*, *36*, 4463–4477.

Slingo, A. (1989), A GCM parameterization for the shortwave radiative properties of clouds, *J. Atmos. Sci.*, *46*, 1419–1427.

Stamnes, K., S.-C. Tsay, W. Wiscombe, and K. Jayaweera (1988), Numerically stable algorithm for discrete-ordinate-method radiative transfer in multiple scattering and emitting layered media, *Appl. Opt.*, *27*(12), 2502–2509.

Stohl, A. (2006), Characteristics of atmospheric transport into the Arctic troposphere, *J. Geophys. Res.*, *111*, D11306, doi:10.1029/2005JD006888.

Thomas, G. E., and K. Stamnes (1999), *Radiative Transfer in the Atmosphere and Ocean*, Cambridge Atmospheric and Space Science Series, Cambridge Univ. Press, New York.

Toon, O. B., C. P. McKay, T. P. Ackerman, and K. Santhanam (1989), Rapid calculation of radiative heating rates and photodissociation rates in inhomogeneous multiple scattering atmospheres, *J. Geophys. Res.*, *94*(D13), 16,287–16,301.

Van der Werf, G. R., J. T. Randerson, L. Giglio, G. J. Collatz, P. S. Kasibhatla, and A. F. Arellano Jr. (2006), Interannual variability of global biomass burning emissions from 1997 to 2004, *Atmos. Chem. Phys.*, *6*, 3423–3441.

Warren, S., and A. Clarke (1990), Soot in the atmosphere and snow surface of Antarctica, *J. Geophys. Res.*, *95*(D2), 1811–1816.

Warren, S., and W. Wiscombe (1980), A model for the spectral albedo of snow. II: Snow containing atmospheric aerosols, *J. Atmos. Sci.*, *37*, 2734–2745.

Warren, S., and W. Wiscombe (1985), Dirty snow after nuclear war, *Nature*, *313*, 467–470.

Warren, S. G., I. G. Rigor, N. Untersteiner, V. F. Radionov, N. N. Bryazgin, Y. I. Aleksandrov, and R. Colony (1999), Snow depth on Arctic sea ice, *J. Clim.*, *12*, 1814–1829.

Wiscombe, W. J., and S. G. Warren (1980), A model for the spectral albedo of snow. I: Pure snow, *J. Atmos. Sci.*, *37*, 2712–2733.

Yang, Z.-L., R. Dickinson, A. Robock, and K. Y. Vinnikov (1997), Validation of snow submodel of the biosphere-atmosphere transfer scheme with Russian snow cover and meteorological observational data, *J. Clim.*, *10*, 353–373.

Zender, C. S., B. Bush, S. K. Pope, A. Bucholtz, W. D. Collins, J. T. Kiehl, F. P. J. Valero, and J. Vitko Jr. (1997), Atmospheric absorption during the atmospheric radiation measurement (ARM) enhanced shortwave experiment (ARESE), *J. Geophys. Res.*, *102*(D25), 29,901–29,915.

Zwally, H. J., W. Abdalati, T. Herring, K. Larson, J. Saba, and K. Steffen (2002), Surface melt-induced acceleration of Greenland ice-sheet flow, *Science*, *297*, 218–222.

M. G. Flanner, J. T. Randerson, and C. S. Zender, Department of Earth System Science, University of California, Irvine, CA 92697-3100, USA. (mflanner@uci.edu)

P. J. Rasch, National Center for Atmospheric Research, Boulder, CO, USA.